Supporting Information for

Near-Perfect CO_2/CH_4 Selectivity Achieved through Reversible Guest Templating in the Flexible Metal–Organic Framework Co(bdp)

Mercedes K. Taylor,[†,‡] Tomče Runčevski,[†,‡] Julia Oktawiec,[†] Jonathan E. Bachman,[§] Rebecca L. Siegelman,[†,‡] Henry Jiang,[†] Jarad A. Mason,[†] Jacob D. Tarver,[∥,⊥] and Jeffrey R. Long[†,‡,§*]

[†]Department of Chemistry, University of California, Berkeley, California 94720, United States

[‡]Materials Sciences Division, Lawrence Berkeley National Laboratory, Berkeley, California 94720, United States

[§]Department of Chemical and Biomolecular Engineering, University of California, Berkeley, California 94720, United States

[∥]NIST Center for Neutron Research, National Institute of Standards and Technology, Gaithersburg, Maryland 20899, United States

[⊥]National Renewable Energy Laboratory, Golden, Colorado 80401, United States

*Correspondence to: jrlong@berkeley.edu

Table of Contents **Page**

General Information

Anhydrous *N,N*-dimethylformamide (DMF) and anhydrous dichloromethane (CH_2Cl_2) were obtained from a JC Meyer solvent system. All other reagents were obtained from commercial vendors and used without further purification. Ultra-high purity (≥99.998% purity) dinitrogen, helium, carbon dioxide, methane, and dihydrogen were used for all adsorption measurements.

Synthesis of Co(bdp)

Co(bdp) was prepared according to a previously published procedure.[1] Specifically, a 100 mL solvent bomb was charged with a magnetic stir bar, $Co(CF_3SO_3)_2$ (0.72 g, 2.0 mmol, 1.1 equiv), H_2bdp (1.9 mmol, 1.0 equiv),[2] and 10 mL of *N,N*-diethylformamide (DEF). The mixture was degassed using five freeze-pump-thaw cycles and then sealed by closing the stopcock of the solvent bomb while the frozen reaction mixture remained under vacuum. The solvent bomb was then heated at 160 °C for 3 d to afford a purple microcrystalline solid. Upon completion of the reaction, the solvent bomb was backfilled with Ar, the supernatant was removed under positive Ar pressure and discarded, and 80 mL of anhydrous *N,N*-dimethylformamide (DMF) was added to the solid product under an Ar atmosphere. The solvent bomb was then sealed under Ar and heated to 110 °C overnight. This solvent-exchange procedure was performed once daily for 7 d to completely remove unreacted starting material from the pores. Subsequently, the DMF was replaced with anhydrous CH_2Cl_2 following the same procedure but without heating. These CH_2Cl_2 exchanges were performed once daily for 3 d to allow activation from a lower-boiling solvent. To activate the material, the CH_2Cl_2 was evaporated under positive Ar pressure until 25 mL of solution remained. The resultant slurry was transferred to a 100 mL Schlenk flask under inert atmosphere, and the CH_2Cl_2 was evaporated over the course of 1 h under a flow of Ar at room temperature. The resultant solid was dried under a flow of Ar at 160 °C for 6 h and then placed under dynamic vacuum at 160 °C overnight. The activated solid was immediately transferred to a glovebox and handled under a dinitrogen atmosphere for all further experiments.

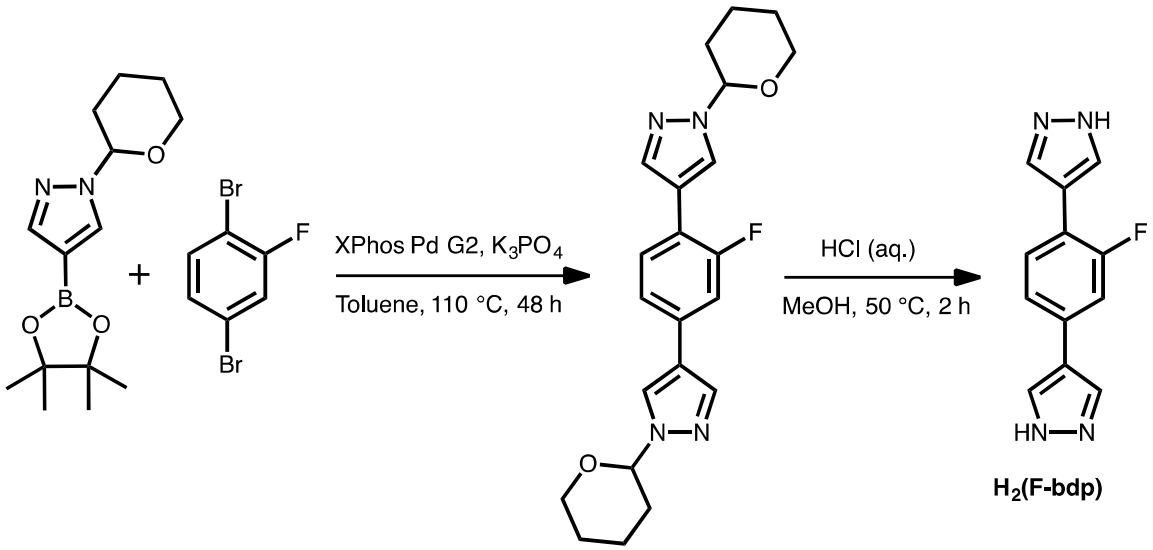

Synthesis of H_2(F-bdp)

H_2(F-bdp) was prepared according to a previously published procedure[3] *via* a Suzuki-Miyaura coupling.[4] Specifically, 1,4-dibromo-2-fluorobenzene (3.03 g, 11.9 mmol, 1.0 equiv), 1-(2-tetrahydropyranyl)-1H-pyrazole-4-boronic acid pinacol ester (8.30 g, 29.8 mmol, 2.5 equiv), and K_3PO_4 (12.7 g, 60 mmol, 5 equiv) were suspended in toluene (24 mL) in a 40-mL glass scintillation vial with a magnetic stir bar and sparged with Ar for 10 minutes. XPhos Pd G2 (1.74 g, 2.4 mmol, 0.2 equiv) was added quickly in air, and vial was briefly purged with Ar, sealed with a PTFE-lined cap, and heated to 110 °C while stirring for 2 days. Upon completion, the reaction mixture was cooled to room temperature, concentrated under reduced pressure, and diluted with 250 mL of diethyl ether. The ether layer was washed 5 times with 250 mL of saturated aqueous $NaHCO_3$ solution, dried over $MgSO_4$, and concentrated under reduced pressure to yield a yellow oil, which was used in the subsequent reaction without additional purification. The crude ligand was dissolved in 90 mL of methanol in a 250-mL round-bottom flask with a magnetic stir bar, 18 mL of concentrated aqueous HCl was added, and the reaction mixture was stirred at 50 °C for 2 h, during which time a yellow precipitate formed. The reaction mixture was filtered, and the filtrate was suspended in water and neutralized with $NaHCO_3$. The precipitate was again isolated by filtration, washed with water, and dried *in vacuo* to yield **H_2(F-bdp)** (1.31 g, 5.8 mmol, 49%) as a beige powder. ^{1}H NMR (400 MHz, DMSO-d_6): δ 8.13 (s, 2H), 8.05 (s, 2H) 7.70 (t, J = 8.2 Hz, 1H), 7.52 (dd, J = 12.8, 1.8 Hz, 1H), 7.46 (dd, J = 8.1, 1.8 Hz, 1H) ppm; ^{13}C NMR (101 MHz, DMSO-d_6): δ 160.65, 158.22, 133.04 (d, J = 9.3 Hz), 128.58 (d, J = 5.0 Hz), 121.77, 120.55, 115.15, 112.79, 112.56 ppm; ^{19}F NMR (376 MHz, DMSO-d_6): δ -114.70 ppm. Note that the ^{1}H NMR signals from the hydrogen atoms bonded to the pyrazole nitrogen atoms are too broad to be visible. Anal. Calcd. for $C_{12}H_9FN_4$: C, 63.15, H, 3.97, N, 24.55; found: C, 61.85, H, 3.99, N, 23.64. IR: 3137(w), 3079 (w), 2935 (m), 2848 (m), 1624 (w), 1587

(m), 1473 (m), 1452 (m), 1374 (m), 1271 (w), 1252 (w), 1230 (w), 1200 (w), 1157 (m), 1111(m), 1038(m), 984 (w), 961 (m), 950 (m), 876 (m), 857 (s), 814 (s), 750 (m), 724 (m), 669 (w), 661 (w), 594 (s), 556 (m), 533 (m), 520 (m), 508 (m), 498 (w), 483 (m), 471 (m), 459 (s), 452 (m) cm^{-1}.

Synthesis of Co(F-bdp)

Co(F-bdp) was prepared according to a previously published procedure.[3] Specifically, a 100-mL solvent bomb was charged with a magnetic stirring bar, $Co(CF_3SO_3)_2$ (0.75 g, 2.1 mmol, 1.0 equiv), H_2(F-bdp) (0.48 g, 2.1 mmol, 1.0 equiv), and DMF (10.4 mL). The reaction mixture was degassed by the freeze–pump–thaw method for 5 cycles, then sealed by closing the stopcock of the solvent bomb while the frozen reaction mixture remained under vacuum. The solvent bomb was then heated at 160 °C for 3 days to afford a purple microcrystalline solid. (To obtain crystals suitable for single-crystal X-ray diffraction, the magnetic stir bar was omitted from reaction flask while maintaining all other conditions constant.) Upon completion, the solvent bomb was backfilled with Ar, the supernatant was removed under positive Ar pressure and discarded, and 80 mL of anhydrous DMF was added to the solid product while maintaining under inert atmosphere. The solvent bomb was then sealed under Ar and heated to 110 °C overnight. This solvent-exchange procedure was performed once daily for 7 days to completely remove unreacted starting material from the pores. Subsequently, the DMF was replaced with anhydrous CH_2Cl_2 following the same procedure but without heating; these CH_2Cl_2 exchanges were performed once daily for 3 days to allow activation from a lower-boiling solvent. To activate the material, the CH_2Cl_2 was removed under positive Ar pressure until 25 mL of solution remained. The resultant slurry was transferred to a 100-mL Schlenk flask under inert atmosphere, and the CH_2Cl_2 was evaporated by flowing Ar at room temperature for 1 h. The resultant solid was dried by flowing Ar at 160 °C for 6 h, then placed under dynamic vacuum at 160 °C overnight to yield **Co(F-bdp)** (0.153 g, 0.5 mmol, 25%). The activated solid was immediately transferred to a glovebox and handled under a dinitrogen atmosphere for all further experiments. Anal. Calcd. for $C_{12}H_9CoFN_4$: C, 50.19, H, 3.16, N, 19.51; found: C, 47.39, H, 2.29, N, 18.29. IR: 1575 (m), 1490 (w), 1442 (w), 1374 (m), 1356 (m), 1331 (m), 1254 (m), 1236 (m), 1198 (w), 1170 (s), 1108 (m), 1079 (w), 1050 (s), 998 (m), 989 (m), 953 (s), 854 (s), 816 (s), 720 (w), 660 (m), 652 (m), 606 (s), 559 (s), 481 (s), 467 (s) cm^{-1}.

Single-Component Adsorption

I. Background adsorption corrections

Background adsorption isotherms were measured using an empty sample holder for H_2, N_2, and CH_4 at all temperatures for which isotherms are reported herein, and all of these background isotherms showed negligible background adsorption. However, when adsorption isotherms were measured for CO_2 using an empty sample holder at the corresponding temperatures, significant background adsorption was observed. This background CO_2 adsorption was fit using 6th-order polynomial functions (Figures S1-S5). These functions were then used to correct the raw CO_2 adsorption data, by subtracting the background adsorption from the measured adsorption at each observed pressure.

II. Complete adsorption and desorption data

The experimental procedure for single-component adsorption measurements is provided in the main text. Variable temperature isotherms for H_2, N_2, and CO_2 adsorption in Co(bdp) are shown in Figures S6-S16. Variable temperature isotherms for CH_4 adsorption in Co(bdp) have already been reported[1], but CH_4 adsorption was measured again at 25 °C on the same Co(bdp) sample used throughout this work to verify reproducibility and sample quality, and this CH_4 adsorption isotherm is shown in Figure S17.

III. Calculation of h_{ads} for CO_2 in Co(bdp)

To obtain the differential enthalpies (h_{ads}) of CO_2 adsorption, the high-pressure CO_2 adsorption isotherms at 0, 12, 25, 40, and 50 °C were first fit with linear splines (Figure S18). Using the isotherm fits, the exact pressures (P) corresponding to specific CO_2 loadings (n) were determined at each temperature (T). The Clausius−Clapeyron relationship was then used to calculate the differential enthalpies of adsorption (h_{ads}) based on the slopes of the linear trendlines fit to ln P vs. 1/T at each value of n in Eq. S1 below. Standard errors were calculated from the deviations of the best-fit lines.

$$(\ln P)_n = \frac{h_{ads}}{RT} + C \qquad Eq.\ S1$$

Multicomponent Equilibrium Adsorption

I. Partial CO_2 and CH_4 pressures of adsorbed phase and headspace

A complete description of the experimental procedure is provided in the main text. In summary, a high-pressure adsorption instrument (HPVA-II-100) and a mass spectrometer (MKS Microvision 2) were used in tandem to analyze the adsorbed gas after Co(bdp) equilibrated under a known mixture of CO_2 and CH_4. An explanation of the data analysis is provided below.

The raw data provided by the HPVA-II-100 are:

- Pressure of dosing manifold + sample holder after equilibration: $\mathbf{P_{eq}}$ (bar)
- Temperature of the manifold ($\mathbf{T_m}$) and temperature of the sample ($\mathbf{T_s}$)

These data are used by the HPVA-II-100 software to calculate the following experimental values:

- Volume of gas in dosing manifold before opening to sample: $\mathbf{V_{dosed}}$ (cc STP)
- Volume of gas adsorbed onto sample after equilibration: $\mathbf{V_{ads}}$ (cc STP)

The raw data provided by the MKS Microvision 2 are:

- Mole fraction CO_2 relative to all gas in the sample holder after equilibration: $\mathbf{x_{CO2}}$
- Mole fraction CH_4 relative to all gas in the sample holder after equilibration: $\mathbf{x_{CH4}}$

Known experimental variables are:

- Sample mass: **m** (g)
- Mole fraction CO_2 dosed: $\mathbf{y_{CO2}}$
- Mole fraction CH_4 dosed: $\mathbf{y_{CH4}}$
- Free space of sample holder: $\mathbf{V_{FS}}$ (cc STP)

The raw data provided by the HPVA-II-100 can be converted to moles using the following equations:

$$\frac{\mathbf{V_{dosed}}}{2.24 \times 10^4 \text{ cc/mol}} = \mathbf{n_{dosed}} \qquad \textit{Eq. S2}$$

$$\frac{\mathbf{P_{eq}} \times \mathbf{V_{FS}}}{(8.314 \times 10^{-5} \text{ cc bar/K mol}) \times \mathbf{T_S}} = \mathbf{n_{headspace}} \qquad \textit{Eq. S3}$$

$$\frac{\mathbf{V_{ads}}}{2.24 \times 10^4 \text{ cc/mol}} = \mathbf{n_{ads}} \qquad \textit{Eq. S4}$$

Figure S19 shows a schematic of the multicomponent adsorption experimental set-up, illustrating $\mathbf{n_{dosed}}$, $\mathbf{n_{headspace}}$, and $\mathbf{n_{ads}}$.

The mole fractions given by the MKS Microvision 2 ($\mathbf{x_{CO2}}$ and $\mathbf{x_{CH4}}$) can be converted to moles ($\mathbf{n_{CO2}}$ and $\mathbf{n_{CH4}}$) as follows.

$\mathbf{x_{CO2}}$ is defined as moles CO_2 divided by moles total gas:

$$\mathbf{x_{CO2}} = \frac{\mathbf{n_{CO2}}}{\mathbf{n_{CO2}} + \mathbf{n_{CH4}}} \qquad \textit{Eq. S5}$$

$\mathbf{x_{CH4}}$ is related to $\mathbf{x_{CO2}}$ according to:

$$\mathbf{x_{CH4}} = 1 - \mathbf{x_{CO2}} \qquad \textit{Eq. S6}$$

The ratio of the mole fractions is equal to the ratio of the molar values:

$$\frac{1 - \mathbf{x_{CO2}}}{\mathbf{x_{CO2}}} = \frac{\mathbf{n_{CH4}}}{\mathbf{n_{CO2}}} \qquad \textit{Eq. S7}$$

We can define this ratio as a constant *k*:

$$\frac{1 - \mathbf{x_{CO2}}}{\mathbf{x_{CO2}}} = k \qquad \textit{Eq. S8}$$

Substituting *k* into Equation S7 gives:

$$k \times \mathbf{n_{CO2}} = \mathbf{n_{CH4}} \qquad \textit{Eq. S9}$$

The total moles of gas are given by the HPVA-II-100 data:

$$\mathbf{n_{CO2}} + \mathbf{n_{CH4}} = \mathbf{n_{headspace}} + \mathbf{n_{ads}} \qquad \textit{Eq. 10}$$

Substituting Equation S9 for $\mathbf{n_{CH4}}$ into Equation S10 gives:

$$\mathbf{n_{CO2}} + (k \times \mathbf{n_{CO2}}) = \mathbf{n_{headspace}} + \mathbf{n_{ads}} \qquad \textit{Eq. S11}$$

Simplifying Equation S11 allows us to solve for $\mathbf{n_{CO2}}$ numerically:

$$\mathbf{n_{CO2}} = \frac{\mathbf{n_{headspace}} + \mathbf{n_{ads}}}{1 + k} \qquad \textit{Eq. S12}$$

Using the value for $\mathbf{n_{CO2}}$ found in Equation S12, Equation S9 can be used to solve numerically for $\mathbf{n_{CH4}}$. The above values can then be used to determine the moles CO_2 and moles CH_4 adsorbed onto Co(bdp) as follows.

$\mathbf{n_{CO2manifold}}$ is defined as the moles CO_2 in the dosing manifold after equilibration:

$$(\mathbf{n_{dosed}} \times \mathbf{y_{CO2}}) - \mathbf{n_{CO2}} = \mathbf{n_{CO2manifold}} \qquad \textit{Eq. S13}$$

$\mathbf{n_{CH4manifold}}$ is defined as the moles CH_4 in the dosing manifold after equilibration:

$$(\mathbf{n_{dosed}} \times \mathbf{y_{CH4}}) - \mathbf{n_{CH4}} = \mathbf{n_{CH4manifold}} \qquad \textit{Eq. S14}$$

$\mathbf{x_{CO2manifold}}$ is defined as the mole fraction of CO_2 in the dosing manifold after equilibration.

$$\frac{\mathbf{n_{CO2manifold}}}{\mathbf{n_{CO2manifold}} + \mathbf{n_{CH4manifold}}} = \mathbf{x_{CO2manifold}} \qquad \textit{Eq. S15}$$

$\mathbf{x_{CO2headspace}}$ is defined as the mole fraction of CO_2 in the headspace of the sample after equilibration, which is necessarily equal to $\mathbf{x_{CO2manifold}}$.

$$\mathbf{x_{CO2manifold}} = \mathbf{x_{CO2headspace}} \qquad \textit{Eq. S16}$$

$\mathbf{x_{CO2headspace}}$ can be converted to moles:

$$\mathbf{x_{CO2headspace}} \times \mathbf{n_{headspace}} = \mathbf{n_{CO2headspace}} \qquad \textit{Eq. S17}$$

$\mathbf{n_{CO2headspace}}$ can be used to find $\mathbf{n_{CH4headspace}}$:

$$\mathbf{n_{headspace}} - \mathbf{n_{CO2headspace}} = \mathbf{n_{CH4headspace}} \qquad \textit{Eq. S18}$$

By substracting the moles CO_2 in the manifold and headspace from the moles CO_2 dosed, we can calculate the moles CO_2 adsorbed onto Co(bdp) ($\mathbf{n_{CO2ads}}$):

$$(\mathbf{n_{dosed}} \times \mathbf{y_{CO2}}) - (\mathbf{n_{CO2manifold}} + \mathbf{n_{CO2headspace}}) = \mathbf{n_{CO2ads}} \qquad \textit{Eq. S19}$$

By substracting the moles CH_4 in the manifold and headspace from the moles CH_4 dosed, we can calculate the moles CH_4 adsorbed onto Co(bdp) ($\mathbf{n_{CH4ads}}$):

$$(\mathbf{n_{dosed}} \times \mathbf{y_{CH4}}) - (\mathbf{n_{CH4manifold}} + \mathbf{n_{CH4headspace}}) = \mathbf{n_{CH4ads}} \qquad \textit{Eq. S20}$$

The partial CO_2 pressure of the headspace at equilibrium can be calculated as follows:

$$\mathbf{x_{CO2headspace}} \times \mathbf{P_{eq}} = \mathbf{P_{CO2}} \qquad \textit{Eq. S21}$$

The partial CH4 pressure of the headspace at equilibrium can be calculated as follows:

$$(1 - \mathbf{x_{CO2headspace}}) \times \mathbf{P_{eq}} = \mathbf{P_{CH4}} \qquad \textit{Eq. S22}$$

II. CO_2/CH_4 selectivity calculations

To determine the CO_2/CH_4 selectivity ($\boldsymbol{\alpha}$) of Co(bdp) under conditions in which a significant amount of CH_4 was adsorbed, the following expression was used:

$$\boldsymbol{\alpha} = \frac{\frac{\mathbf{n_{CO2ads}}}{\mathbf{n_{CH4ads}}}}{\frac{\mathbf{n_{CO2headspace}}}{\mathbf{n_{CH4headspace}}}} \qquad \textit{Eq. S23}$$

For comparison to the experimentally-determined selectivity value of 61 ± 4 discussed in the main text, the theoretical CO_2/CH_4 selectivity under CH_4-rich conditions was calculated from single-component CO_2 and CH_4 adsorption isotherms. The data points used from each adsorption isotherm were (3.62 bar CO_2, 3.39 mmol CO_2/g) and 55.64 bar CH_4, 9.15 mmol CH_4/g), respectively. Plugging these values into Eq. S23 yields a CO_2/CH_4 selectivity of 5.7, significantly smaller than the selectivity determined under multicomponent equilibrium conditions. This discrepancy further highlights the importance of using multicomponent equilibrium measurements to study gas separations in flexible metal–organic frameworks.

III. Multicomponent compressibility factors

A compressibility factor is a correction used to describe the extent to which a gas deviates from ideal gas behavior, as shown in Equation S24.[5]

$$\mathrm{Z} = \frac{\mathrm{PV}}{\mathrm{RT}} \qquad \textit{Eq. S24}$$

It is necessary to use compressibility factors in the data analysis of volumetric adsorption experiments, which rely on the change in volume of a gas to determine the amount adsorbed by a sample. The compressibility factor of a certain pure gas or gas

mixture can be obtained from the NIST REFPROP database[6] for a given pressure and temperature. In all single-component adsorption experiments reported herein, the appropriate compressibility factors were used by the HPVA-II-100 software to calculate the volume of that gas adsorbed by the sample.

In the case of multicomponent adsorption experiments, the starting ratio of components is known and can be used to obtain the corresponding compressibility factor from the NIST REFPROP database.[6] However, the final ratio of components in the headspace (after equilibration with the sample) is not known, because the sample may show selectivity for one component over the other. Our experimental set-up made it necessary to choose equilibrium compressibility factors without knowing the equilibrium composition of the headspace, because the determination of this composition via the mass spectrometry data requires knowledge of the total amount of gas adsorbed (See Part I of the Multicomponent Adsorption Data Analysis section of the Supporting Information). Therefore, we made the conservative estimate that Co(bdp) would show no selectivity for CO_2 or CH_4, and we used compressibility factors corresponding to the starting ratio of components for all steps of the multicomponent adsorption calculations performed by the HPVA-II-100 software, both before and after equilibration.

To verify that this choice of compressibility factors is valid, we performed the adsorption calculations for the same mixed gas experiment three times, using three different assumptions:

1) That Co(bdp) shows no CO_2 or CH_4 selectivity, leaving the equilibrium headspace composition equal to the starting headspace composition
2) That Co(bdp) shows perfect CO_2 selectivity and adsorbs only CO_2, leaving the equilibrium headspace enriched in CH_4 relative to the starting headspace composition
3) That Co(bdp) shows perfect CH_4 selectivity and adsorbs only CH_4, leaving the equilibrium headspace enriched in CO_2 relative to the starting headspace composition

This analysis was performed on the highest-pressure data point of Figure 2, in which Co(bdp) was dosed with a 50:50 mixture of CO_2:CH_4. To perform adsorption calculations based on Assumption 1, equilibrium compressibility factors were used that correspond to a 50:50 mixture of CO_2:CH_4 (since the starting ratio is unchanged in this scenario). These calculations yield a total adsorption value of **11.1 mmol/g**, which is shown in Figure 2.

To perform adsorption calculations based on Assumption 2, we estimated the theoretical maximum CO_2 capacity at this CO_2 partial pressure using the pure CO_2 isotherm shown in Figure 1b. In the mixed-gas experiment in question, Co(bdp) equilibrated under 25.25 bar of a 50:50 mixture of CO_2:CH_4, which corresponds to a partial CO_2 pressure of 12.63 bar. At this point (12.63 bar) on the pure CO_2 isotherm,

Co(bdp) adsorbs 10.2 mmol/g of CO_2. If Co(bdp) were to exhibit this same CO_2 capacity in the mixed-gas experiment, it would result in an equilibrium headspace CO_2:CH_4 ratio of 44:56. This ratio was used to obtain equilibrium compressibility factors, which yield a total adsorption value of **11.2 mmol/g**. This value (which assumes perfect CO_2 selectivity) is only 1% greater than the value obtained using the conservative Assumption 1 (which assumes *no* selectivity), indicating that our choice to use Assumption 1 to determine equilibrium compressibility factors is valid and that variations in the equilibrium compressibility factors do not distort the data.

We also performed adsorption calculations based on Assumption 3. This assumption is the least plausible, as it assumes Co(bdp) will adsorb only CH_4 and not CO_2, even though Co(bdp) is not even porous at the corresponding point on the pure CH_4 isotherm (Figure 1). Indeed, the assumption that Co(bdp) is perfectly CH_4 selective is incompatible with our body of experimental evidence. However, for the sake of completeness, we obtained compressibility factors using the assumption that Co(bdp) adsorbed 10.2 mmol CH_4/g (the same amount of gas as in Assumption 2). This hypothetical CH_4 capacity would result in an equilibrium headspace CO_2:CH_4 ratio of 56:44, and the corresponding compressibility factors yield a total adsorption value of **10.2 mmol/g**. This value is only 7% less than the value obtained using Assumption 1, which again upholds the validity of our chosen equilibrium compressibility factors.

IV. Error for 6:94 CO_2:CH_4 experiment:

To verify the reproducibility of our experimental design, we repeated the 6:94 CO_2:CH_4 multicomponent adsorption experiment with the same target dosing pressure, and obtained a very similar result in terms of total mixed-gas adsorbed, as shown by the diamonds in Figure S20. For each of the 6:94 CO_2:CH_4 experiments, we also analyzed the gas mixture twice by mass spectrometry, and we used these results to calculate a standard error for each experiment (Figure S21). Although we did not perform multiple mass spectrometry and/or adsorption trials for all of the gas mixtures reported in Figure 2, the error bars shown in Figure S21 give a general picture of the error associated with the multicomponent equilibrium measurements.

Powder X-ray Diffraction

The experimental conditions of powder X-ray diffraction data collection are provided in the main text. The crystal structure analyses (indexing, solution and refinement) were performed with the program TOPAS 4.1[7]. Pattern indexing of the powder X-ray diffraction pattern of evacuated Co(bdp), accomplished *via* the the singular value decomposition method[8], indicated a unit cell similar to that previously published for the evacuated phase of Co(bdp)[1]. When the space group was assigned as C2/c and Pawley refinement attempted using the data, the precise unit cell lattice parameters matched very closely to reported values. In addition, Rietveld refinement using the published structure of evacuated Co(bdp) gave an excellent fit to the experimental data, as shown in Figure S22, confirming that the evacuated Co(bdp) sample used in this study is isostructural to the published model. Figures of merit are presented in Table S1.

After dosing to 3.6 bar of carbon dioxide, the sample adopted the structure of the first CO_2-expanded phase, which remained unchanged upon further dosing to 5.2 bar as evidenced by absence of changes in the collected scattered X-ray intensity (see Figure 3a). This powder diffraction pattern was selected for crystal structure solution and refinement. The pattern indexing was done with the singular value decomposition method[8], resulting in a monoclinic unit cell. Based on the observed reflections, the space group was assumed to be *C*2/*c*, which was later confirmed by the Rietveld refinement. A Pawley fit[9] determined precise unit cell lattice and peak profile parameters, which were used for the crystal structure solution.

The crystal structure of the first CO_2-expanded phase was solved by the global optimization method of simulated annealing (SA) in real space[10]. Considering the *C*2/*c* space group symmetry and the unit cell parameters, one cobalt atom was placed at a special position with multiplicity of 4, where the *x* and *z* fractional coordinates were set to 0 and 1/4, respectively; whereas the *y* fractional coordinate was set as a variable. One half of the ligand was described as a rigid body in a *z* matrix notation (Figure S23), and the other half was created by a symmetry operation imposed by the space group symmetry. During the SA runs, the three rotations, three translations, and the torsion angle of the rigid body were set flexible. The carbon dioxide molecule was described as a single rigid body in a *z* matrix notation, which was freely rotated and translated during the SA runs. The occupancy factors of the linker atoms, and the cobalt atom, were set to 1, whereas the occupancy factors of the carbon dioxide atoms were varied as a single parameter. An overall thermal displacement factor for each rigid body, and the cobalt atom, were included as variables in the SA process within expected limits.

Once a global minimum was found, the crystal structure was subjected to Rietveld refinement[11], in which bond lengths and angles were refined within the rigid bodies, together with free refinement of all profile and lattice parameters, as well as the *y* fractional coordinate of the cobalt atom. The refinement converged quickly, with the figures of merit presented in Table S2. The final Rietveld plot is presented in Figure S24.

Hydrogen atoms were added at calculated positions by the program Mercury [12]. Crystallographic details are provided in the deposited CIF. It is noted that this material displays a high degree of strain, visible in the broadness and paracrystallinity of the peaks in the X-ray diffraction pattern. As a result, the refinement resulted in low precision on the C-C bonds of the structural model. While this is not ideal, the values obtained are reasonable given the limitations of the data.

The same procedure was repeated for the sample collected at 7.2 bar gas pressure of 50:50 CO_2:CH_4. The crystal structure was found to be identical to that of the first CO_2-expanded phase described above (Figure 3d). The final Rietveld plot is presented in Figure S25. Crystallographic details are identical to the deposited CIF.

Additionally, powder X-ray diffraction patterns of Co(bdp) obtained under 11.7 bar of pure carbon dioxide gas and 14.9 bar of 50:50 CO_2:CH_4 were analyzed. While structural determination was ultimately unsuccessful, pattern indexing was done with the singular value decomposition method[8], resulting in a monoclinic unit cell. The space group was assumed to be *C*2/*c*, and Pawley refinements[9] were used to determine the precise unit cell lattice and peak profile parameters for the two powder X-ray diffraction patterns (Table S1; Figures S26-S27).

Breakthrough Experiments

Breakthrough experiments were conducted with Co(bdp) as a microcrystalline powder due to difficulty in forming pellets capable of withstanding the large volume change of the framework upon adsorption. A 6" stainless-steel column (0.25" OD, wall thickness 0.035") was packed with 0.51 g of activated Co(bdp) in a nitrogen-filled glovebox. The final length of packed material was approximately 3", and the remaining column volume was filled loosely with glass wool to allow room for adsorption-induced expansion of Co(bdp). The final packed volume of material was approximately 1.25 cm^3. The column was sealed with VCR fittings using 2 μm fritted, stainless steel gaskets and was then attached to a U-shaped piece of stainless-steel tubing fitted with quarter-turn Swagelok plug valves. The column was removed from the glovebox and attached to a manifold consisting of a minimum volume of 1/8" copper tubing fed by four individual Parker-Porter mass flow controllers. The manifold was purged with He through a bypass line before opening the adsorbent column to the manifold. (Note that Co(bdp) degrades upon exposure to humid air.) The U-shaped column was kept in a 4 L water bath at room temperature (22(1) °C).

An SRI Instruments 8610V GC with a 6' Haysep-D column and a thermal conductivity detector (TCD) was used to monitor the breakthrough profile at 1 min intervals. The TCD was calibrated using a series of pre-mixed, Certified Standard tanks of varying percent CO_2 (10, 50, and 90%) in CH_4 as well as pure, research-grade CO_2 and CH_4. A total inlet flow rate of 5 standard cubic centimeters per minute (sccm) or 15 sccm was used for all experiments, as specified in the figure captions. Flow rates were validated using an Agilent ADM Universal Flow Meter and were monitored every 0.5 s at the GC outlet over the course of each experiment. A Swagelok KPB series back-pressure regulator was placed between the column outlet and GC inlet to control the column pressure. An Ashcroft DG25 digital pressure gauge was placed at the column inlet to determine the pressure drop across the column. Activation between breakthrough experiments was performed under a flow of 5 sccm of He at room temperature (22(1) °C) and atmospheric pressure for 12 h. The system deadspace was estimated by measuring the initial breakthrough time of Ar (a non-adsorbing probe gas) on a column pre-equilibrated under He with equivalent experimental conditions. Prior to each experiment, the column was equilibrated under He at the experimental temperature (22 °C) and pressure (1 bar or 7 bar absolute pressure, as specified in the figure captions). To begin each experiment, He flow to the column was stopped as a flow of 50% CO_2 in CH_4 was simultaneously switched to the column inlet. Following complete breakthrough of CO_2, the capacity of each gas (q_i, mmol/g) was determined using the following formula:

$$q_i = \left[\frac{Q}{22.414\,\frac{cc_{STP}}{mmol}}\left(\int_0^t\left(1-\frac{F_i}{F_{0,i}}\right)dt - t_{0,\mathrm{Ar}}\right) - \varepsilon V\left(\frac{y_i P}{RT}\right)\right]\left(\frac{y_i}{m}\right)$$

Here, Q is the average total flow rate in sccm, t is the corrected time in min, F_i is the molar flow rate of species i at time t, $F_{0,i}$ is the inlet molar flow rate of species i, ε is the interparticle void fraction, V is the volume of pelletized adsorbent in cm^3, $t_{0,Ar}$ is the initial breakthrough time of Ar under equivalent experimental conditions, y_i is the mole fraction of species i, P is the total pressure, R is the universal gas constant, T is the column temperature during the experiment, and m is the mass of adsorbent. The interparticle void fraction ε is calculated as

$$\varepsilon = 1 - \frac{\rho_{bulk}}{\rho_{particle}}$$

where ρ_{bulk} is the bulk density in kg/m^3, calculated as m/V = 408 kg/m^3, and $\rho_{particle}$ is the particle density in kg/m^3, estimated as 774 kg/m^3, the previously reported crystallographic density of Co(bdp)[1]. The term corresponding to the void volume accounted for <0.5% of the total adsorbed gas in a typical experiment in this work.

Breakthrough data are shown in Figures S30–S34. For experiments at 7 bar absolute pressure, significant back-mixing was observed in the column. To quantify and correct for this, Ar was used as a non-adsorbing probe gas to collect breakthrough curves under equivalent conditions (Figure S31). In this case, the CO_2 and CH_4 capacities were instead calculated by subtracting the integrated breakthrough time for Ar from that of each adsorbate under equivalent experimental conditions:

$$q_i = \left[\frac{Q}{22.414\frac{cc_{STP}}{mmol}}\left(\int_0^t\left(1-\frac{F_i}{F_{0,i}}\right)dt - \int_0^t\left(1-\frac{F_{\mathrm{Ar}}}{F_{0,\mathrm{Ar}}}\right)dt\right) - \varepsilon V\left(\frac{y_i P}{RT}\right)\right]\left(\frac{y_i}{m}\right)$$

A CO_2 breakthrough capacity of 3.0 ± 0.3 mmol/g was calculated from the experiment performed under 15 sccm of 50:50 CO_2:CH_4 at 7 bar absolute pressure and 22 °C (shown in Figure S30). The low GC scan resolution (1 scan per min), back-mixing, and small sample volume led to large uncertainties on the order of ±0.3 mmol/g in the calculated CO_2 capacities. The CH_4 breakthrough capacity was within error of zero following correction from the Ar breakthrough curve collected under equivalent conditions. Therefore the breakthrough experiments yielded the same result as the equilibrium experiments in the main text: Co(bdp) selectively adsorbs CO_2 and negligible CH_4 from a 50:50 CO_2:CH_4 mixture at 7 bar.

The unusual CO_2 breakthrough profile observed in Figures S30 and S33 results from the inability of Co(bdp) to capture CO_2 at partial pressures below the first CO_2 phase transition pressure (~2 bar at 22 °C, or 29% of the total pressure). This phenomenon has been discussed previously for other flexible frameworks[13]. To control amount of CO_2 in the product stream, the temperature at which the breakthrough separation is performed can be varied, as the pressure at which the first CO_2-induced

phase change occurs has a strong temperature dependence (Figure 4a in the main text). Alternatively, the position of the CO_2-induced step can be controlled by functionalization of the bdp^{2-} linker (Figure 5 of the main text).

Table S1. Crystallographic parameters for evacuated Co(bdp) and for gas-dosed phases. Experimental conditions, unit cell parameters and figures-of-merit as determined by Rietveld and Pawley refinement using powder X-ray diffraction patterns of evacuated Co(bdp), as well as Co(bdp) dosed with pure CO_2 gas and a 50:50 mixture of CO_2:CH_4 at 11.7 bar and 14.9 bar, respectively.

	Evacuated Co(bdp)	Co(bdp) dosed with 11.7 bar CO_2	Co(bdp) dosed with 14.9 bar CO_2/CH_4
λ (Å)	0.45336	0.45336	0.45336
Temp. (K)	298 K	298 K	298 K
Space Group	*C*2/*c*	*C*2/*c*	*C*2/*c*
a (Å)	24.838(6)	22.514(12)	22.577(8)
b (Å)	6.7527(11)	14.056(7)	13.953(4)
c (Å)	7.1380(13)	7.006(4)	6.980(2)
β (º)	92.41(2)	96.14(4)	96.32(2)
V (Å^3)	1196.2(4)	2204(2)	2185.5(11)
R_{wp}	11.31%	7.69%	7.01%
R_{exp}	2.61%	2.02%	1.99%
R_{Bragg}	4.20%	0.90%	4.10%
R_p	8.46%	4.32%	4.30%
GoF	4.34	3.81	3.52

Table S2. Crystallographic parameters for solved structures. Experimental conditions, unit cell parameters and figures-of-merit as determined by Rietveld refinement of crystal structures against the powder X-ray diffraction patterns of Co(bdp) dosed with pure CO_2 gas and a 50:50 mixture of CO_2:CH_4 at 3.6 bar and 7.2 bar, respectively. These two patterns can be fit to isostructural, partially-expanded phases (Figure 3d).

	Co(bdp) dosed with 3.6 bar of CO_2	Co(bdp) dosed with 7.2 bar CO_2/CH_4
λ (Å)	0.45336	0.45336
Temp. (K)	298 K	298 K
Space Group	*C*2/*c*	*C*2/*c*
a (Å)	24.701(7)	24.700(6)
b (Å)	8.211(3)	8.211(2)
c (Å)	7.089(19)	7.089(17)
β (º)	90.26(5)	90.24(4)
V (Å^3)	1437.9(7)	1437.7(6)
R_{wp}	10.82%	10.00%
R_{exp}	2.56%	2.50%
R_{Bragg}	2.57%	2.09%
R_p	7.55%	6.65%
GoF	4.23	4.01

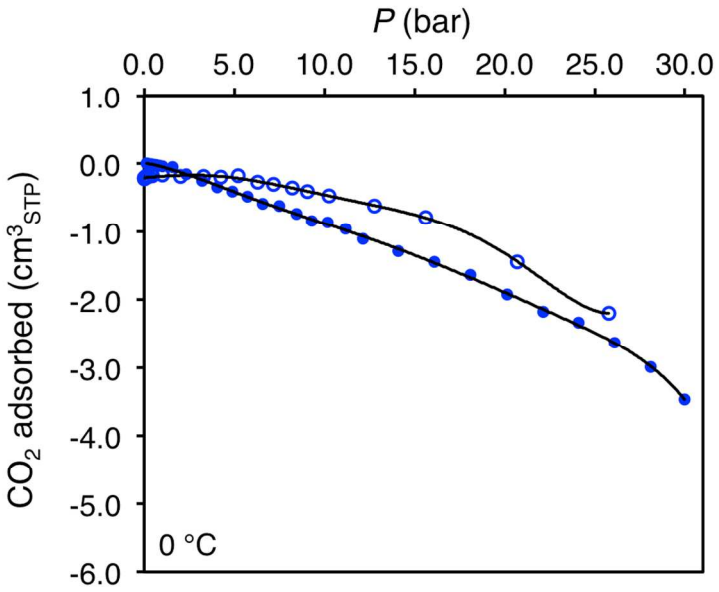

Figure S1. Background CO_2 adsorption at 0 °C. Background CO_2 adsorption was measured with an empty sample holder at 0 °C. Closed circles represent adsorption, open circles represent desorption, and black lines are polynomial fits of the data.

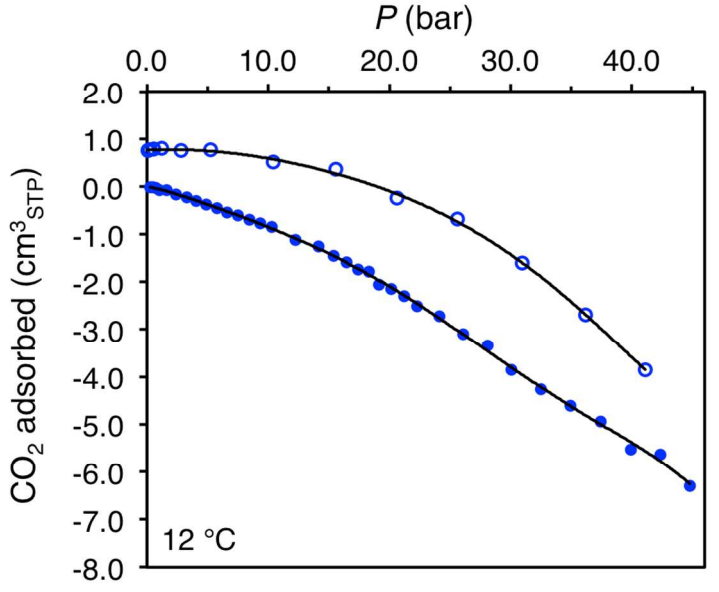

Figure S2. Background CO_2 adsorption at 12 °C. Background CO_2 adsorption was measured with an empty sample holder at 12 °C. Closed circles represent adsorption, open circles represent desorption, and black lines are polynomial fits of the data.

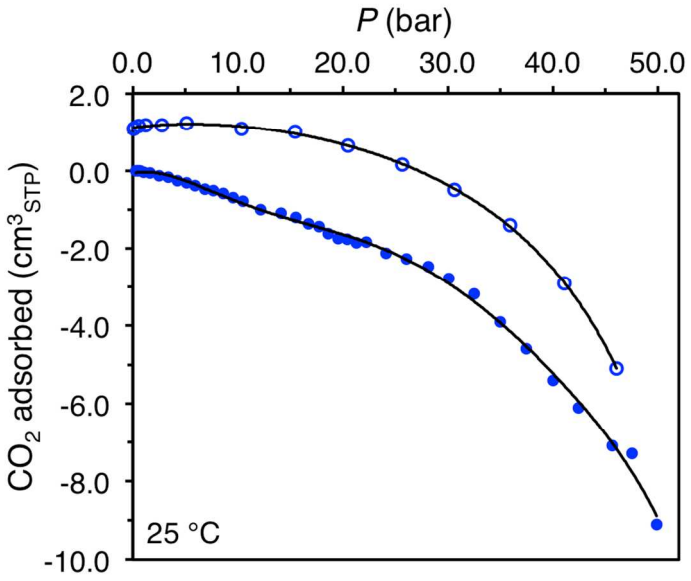

Figure S3. Background CO_2 adsorption at 25 °C. Background CO_2 adsorption was measured with an empty sample holder at 25 °C. Closed circles represent adsorption, open circles represent desorption, and black lines are polynomial fits of the data.

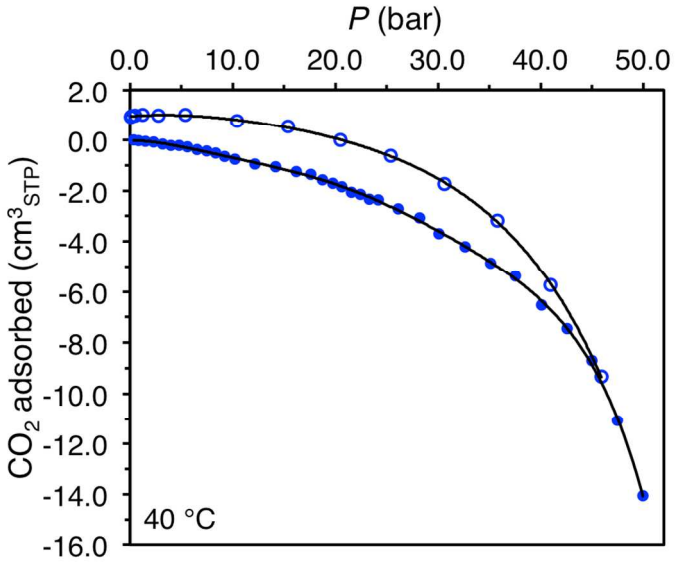

Figure S4. Background CO_2 adsorption at 40 °C. Background CO_2 adsorption was measured with an empty sample holder at 40 °C. Closed circles represent adsorption, open circles represent desorption, and black lines are polynomial fits of the data.

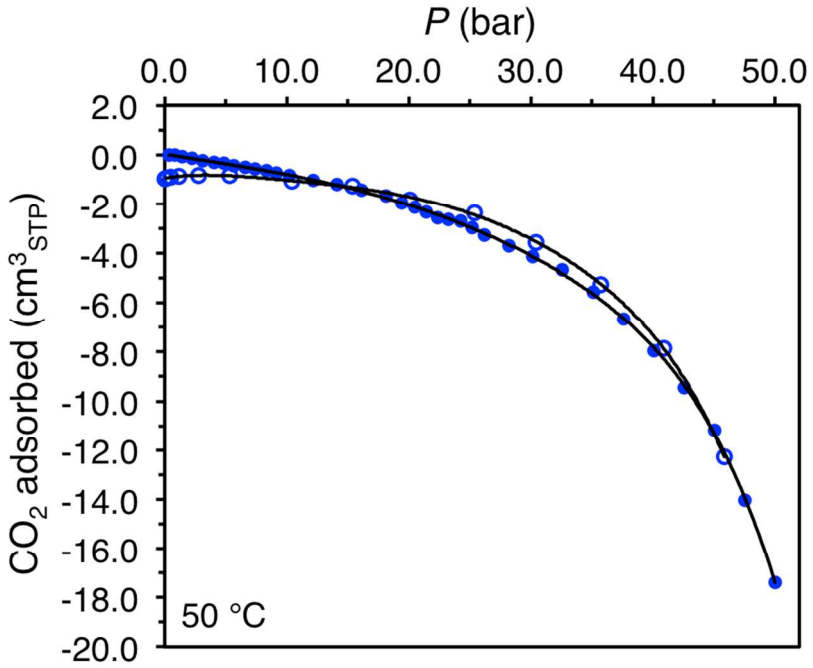

Figure S5. Background CO_2 adsorption at 50 °C. Background CO_2 adsorption was measured with an empty sample holder at 50 °C. Closed circles represent adsorption, open circles represent desorption, and black lines are polynomial fits of the data.

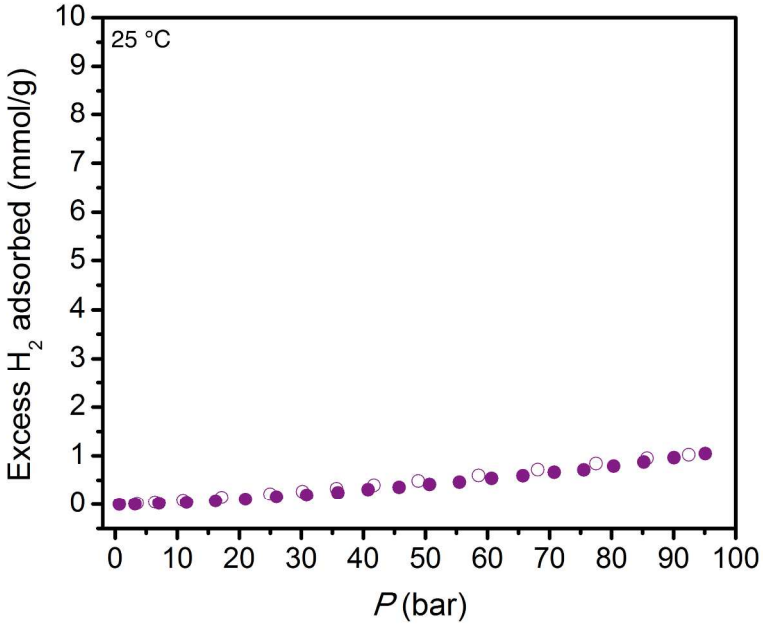

Figure S6. H_2 adsorption in Co(bdp). H_2 adsorption (closed circles) and desorption (open circles) was measured at 25 °C in Co(bdp).

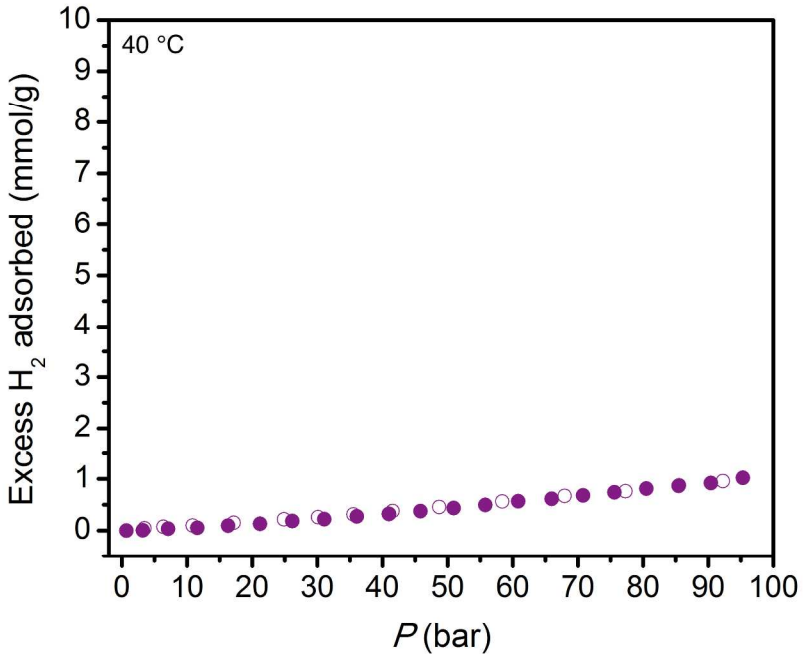

Figure S7. H_2 adsorption in Co(bdp). H_2 adsorption (closed circles) and desorption (open circles) was measured at 40 °C in Co(bdp).

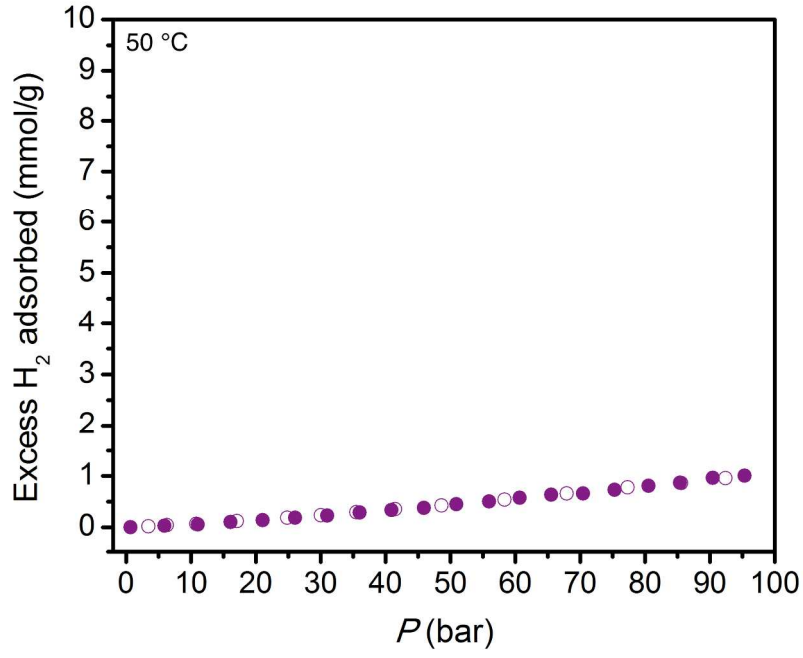

Figure S8. H_2 adsorption in Co(bdp). H_2 adsorption (closed circles) and desorption (open circles) was measured at 50 °C in Co(bdp).

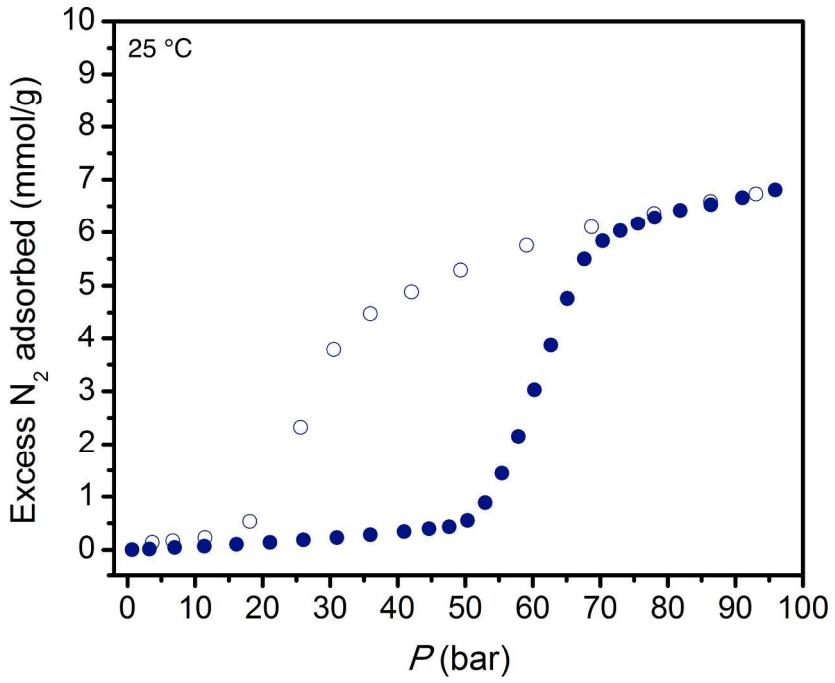

Figure S9. N_2 adsorption in Co(bdp). N_2 adsorption (closed circles) and desorption (open circles) was measured at 25 °C in Co(bdp).

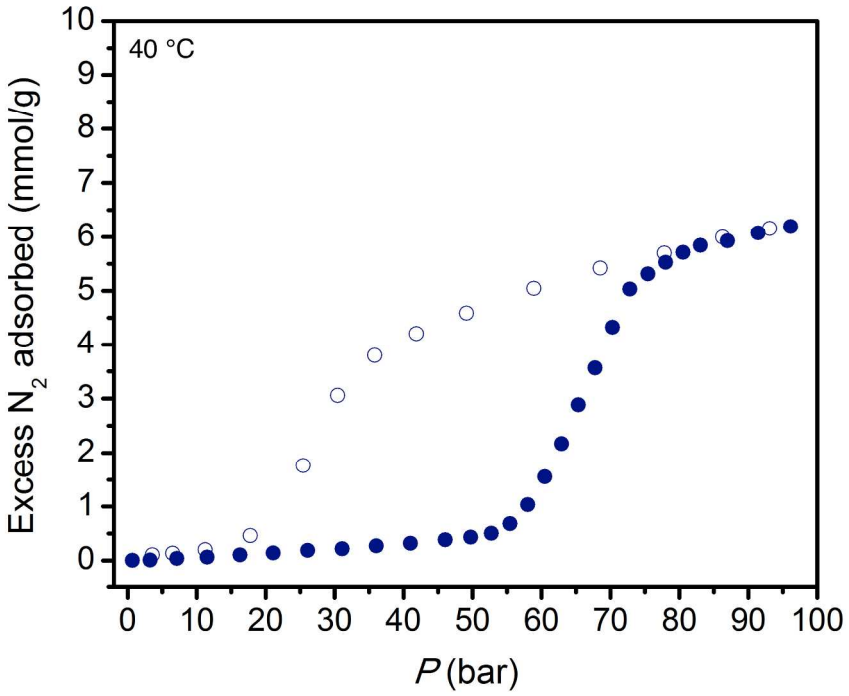

Figure S10. N_2 adsorption in Co(bdp). N_2 adsorption (closed circles) and desorption (open circles) was measured at 40 °C in Co(bdp).

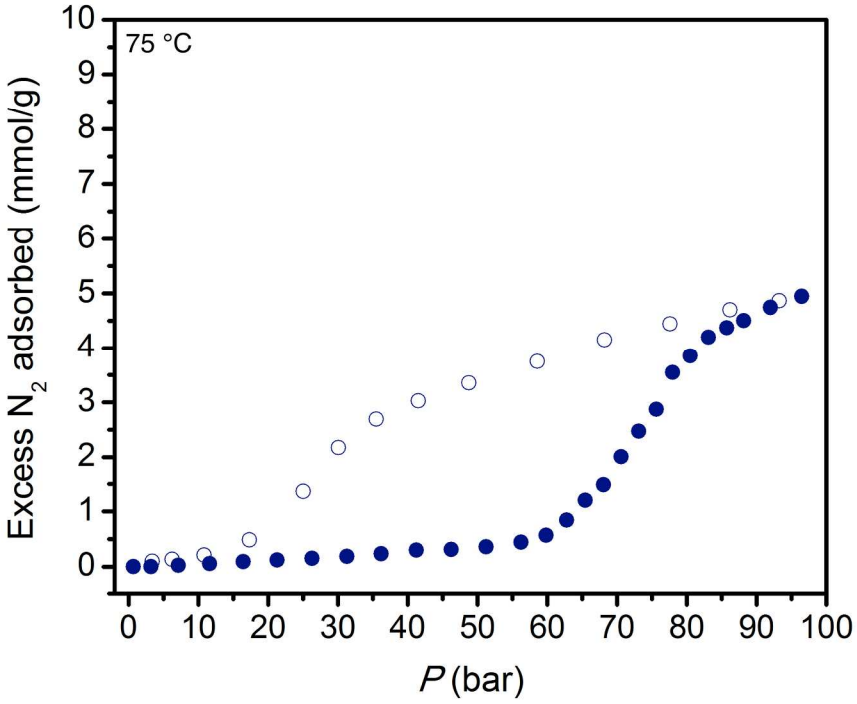

Figure S11. N_2 adsorption in Co(bdp). N_2 adsorption (closed circles) and desorption (open circles) was measured at 75 °C in Co(bdp).

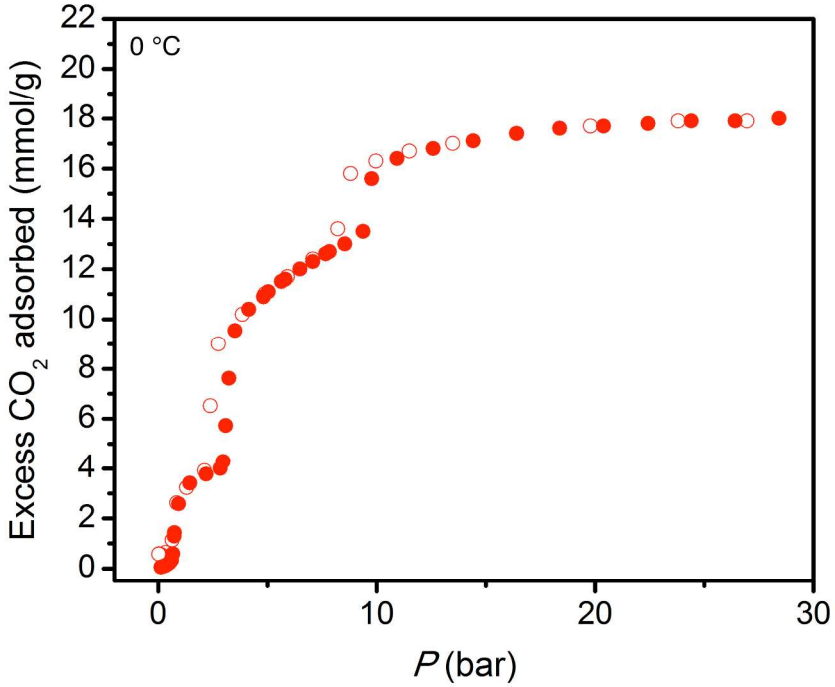

Figure S12. CO_2 adsorption in Co(bdp). CO_2 adsorption (closed circles) and desorption (open circles) was measured at 0 °C in Co(bdp).

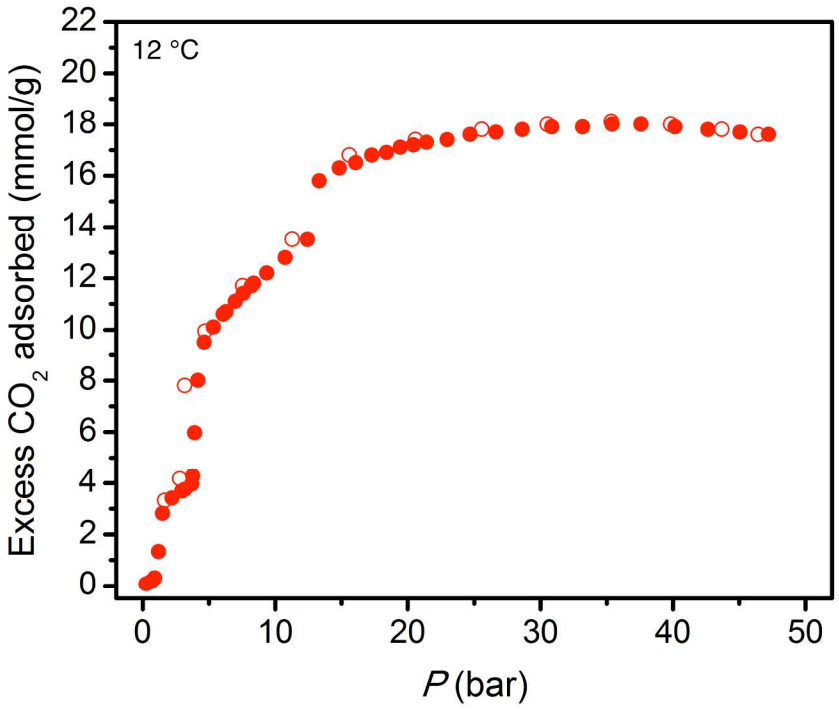

Figure S13. CO_2 adsorption in Co(bdp). CO_2 adsorption (closed circles) and desorption (open circles) was measured at 12 °C in Co(bdp).

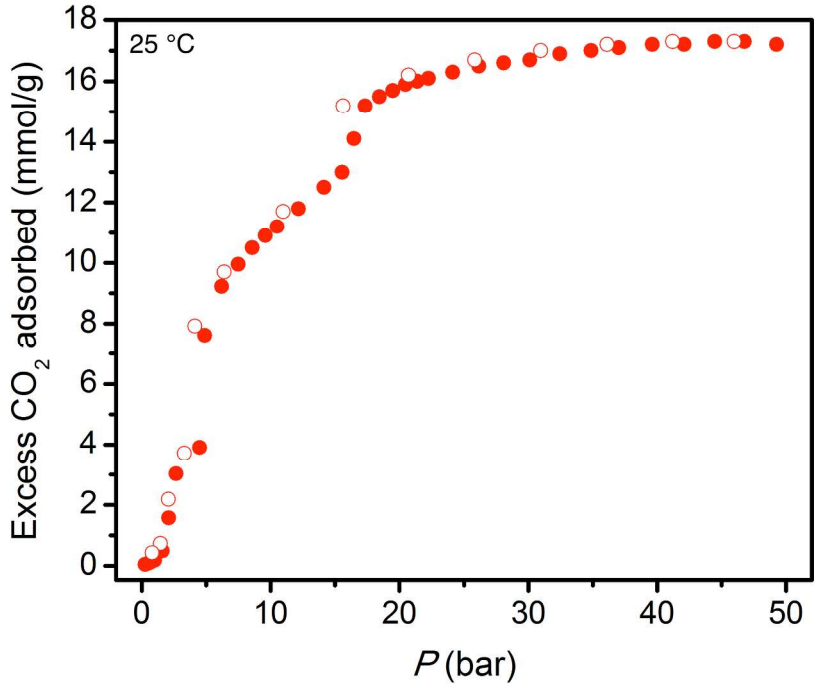

Figure S14. CO_2 adsorption in Co(bdp). CO_2 adsorption (closed circles) and desorption (open circles) was measured at 25 °C in Co(bdp).

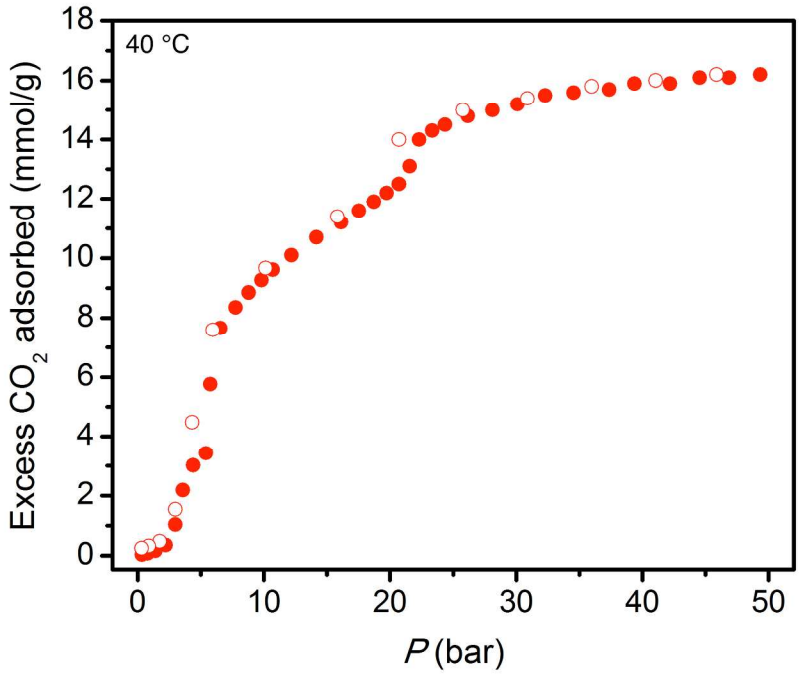

Figure S15. CO_2 adsorption in Co(bdp). CO_2 adsorption (closed circles) and desorption (open circles) was measured at 40 °C in Co(bdp).

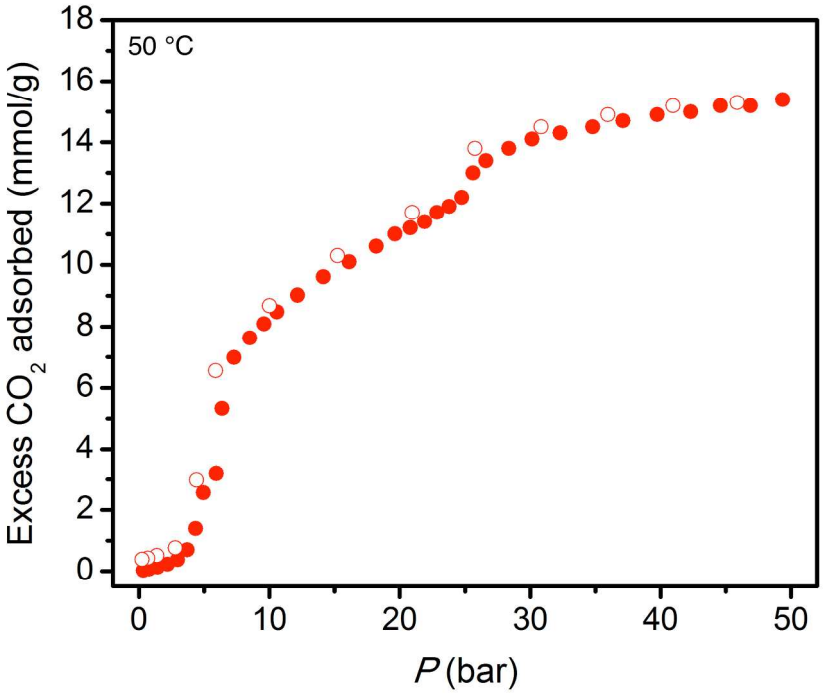

Figure S16. CO_2 adsorption in Co(bdp). CO_2 adsorption (closed circles) and desorption (open circles) was measured at 50 °C in Co(bdp).

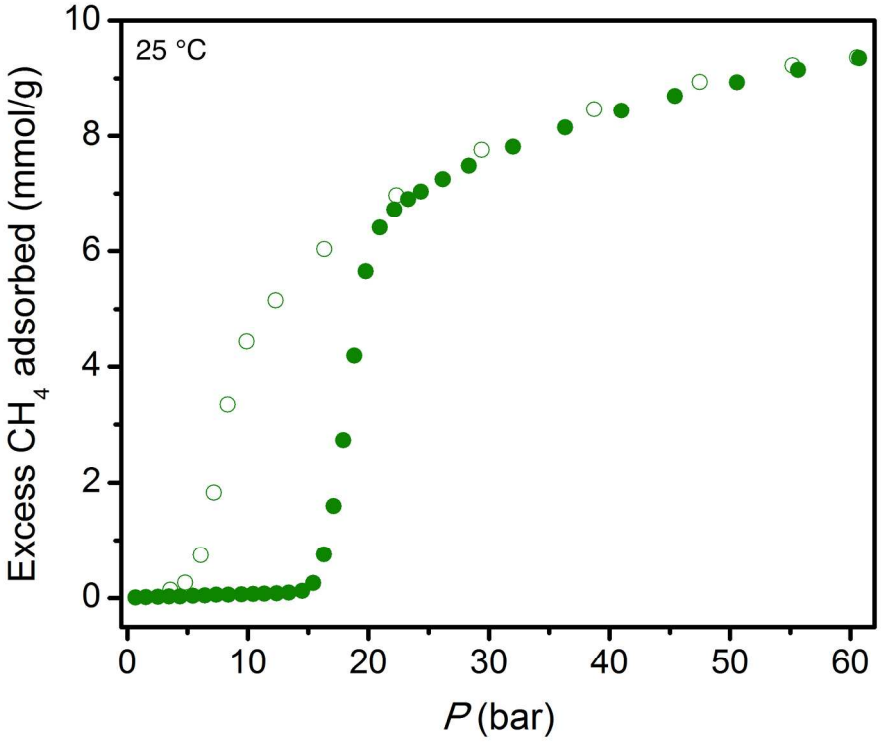

Figure S17. CH_4 adsorption in Co(bdp). CH_4 adsorption (closed circles) and desorption (open circles) was measured at 25 °C in Co(bdp).

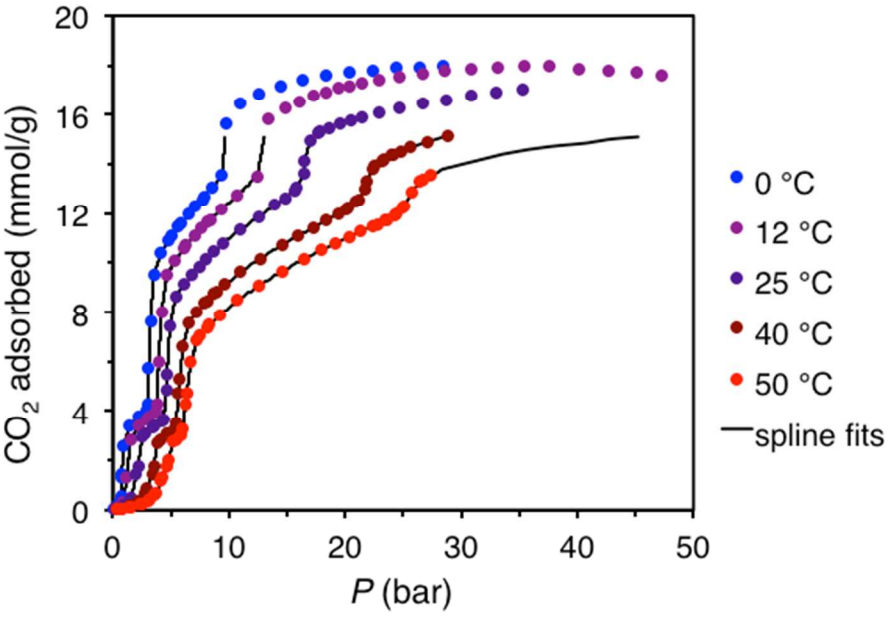

Figure S18. CO_2 isotherm fits. CO_2 adsorption isotherms for Co(bdp) at 0, 12, 25, 40, and 50 °C, along with the corresponding spline fit for each isotherm.

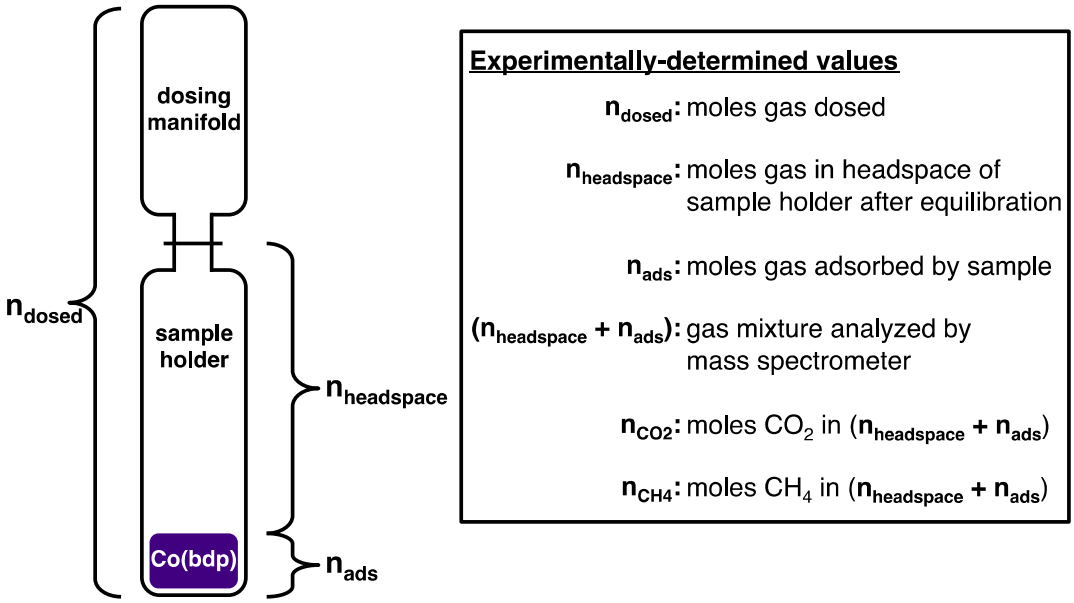

Figure S19. Multicomponent adsorption system. A schematic of the dosing manifold and sample holder, with a summary of experimentally-determined values.

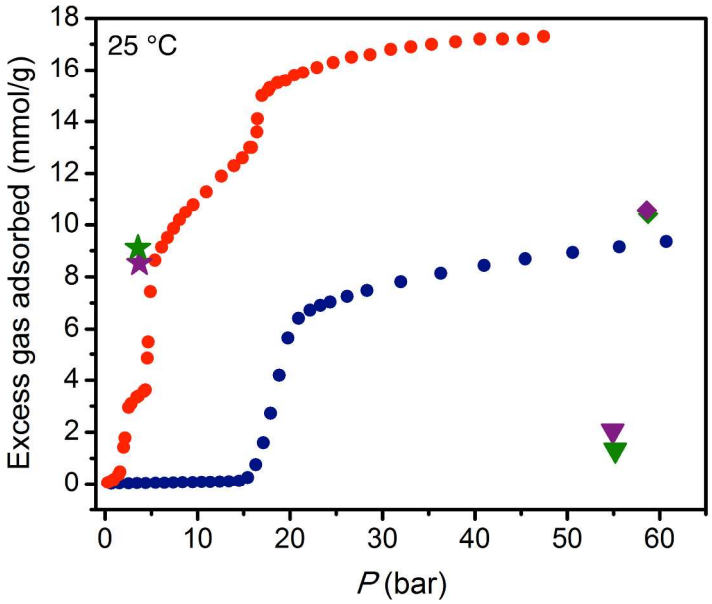

Figure S20. 6:94 CO_2:CH_4 multicomponent adsorption experiments. The 6:94 CO_2:CH_4 adsorption experiment was repeated to verify reproducibility (purple and green symbols represent the first and second trials, respectively), yielding very similar results for total mixed-gas adsorption (diamonds). Stars represent CO_2 adsorption and triangles represent CH_4 adsorption.

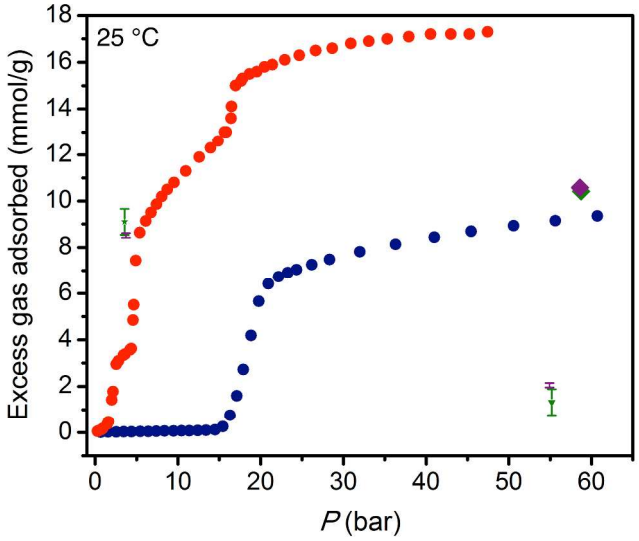

Figure S21. Error in multicomponent adsorption data. Each gas mixture resulting from the two 6:94 CO_2:CH_4 adsorption experiments depicted in Figure S2 was analyzed twice by mass spectrometry, which allowed us to calculate the standard error for CO_2 and CH_4 adsorption for each experiment.

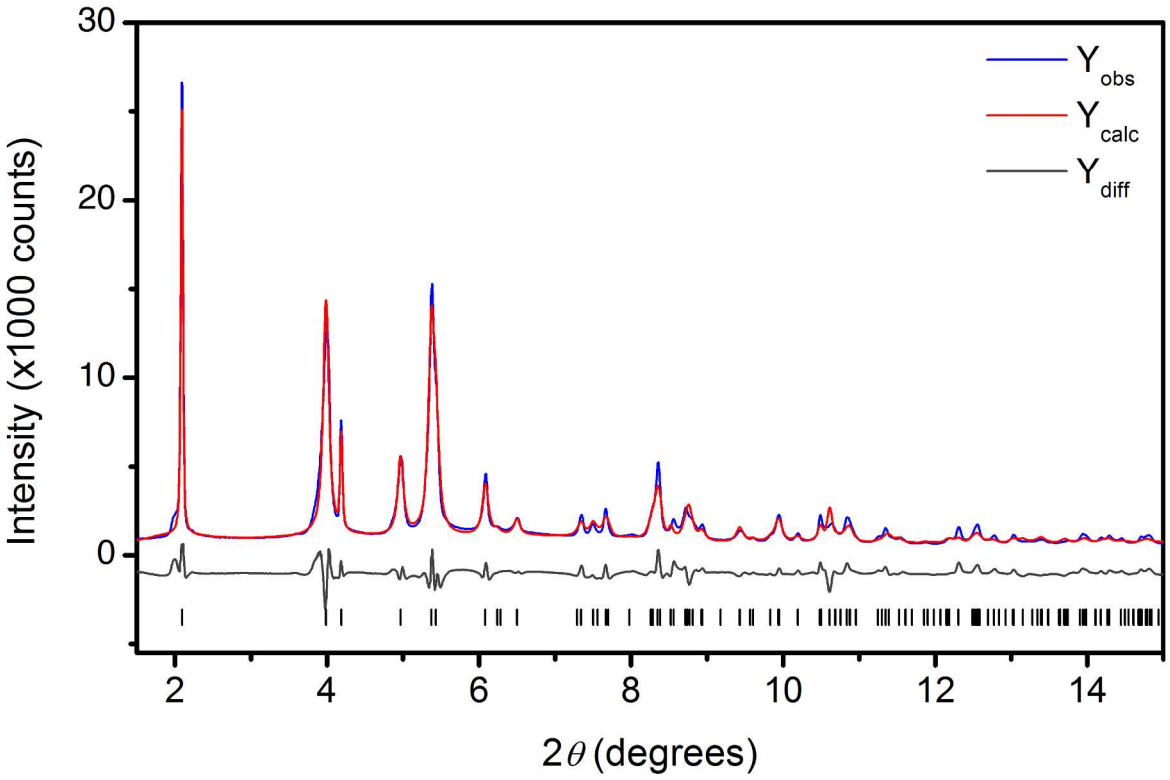

Figure S22. Rietveld refinement of evacuated Co(bdp). The Rietveld refinement of a sample of Co(bdp) at 0 bar and 298 K from 1.5º to 15º using the previously published structural model for evacuated Co(bdp)[1] gives an excellent fit to the experimental data. Blue and red lines represent the observed and calculated diffraction patterns, respectively. The gray line represents the difference between observed and calculated patterns, and the black tick marks indicate calculated Bragg peak positions. Figures-of-merit (as defined by TOPAS): R_{wp} = 11.31%, R_p = 8.46%, R_{exp} = 2.61%, R_{Bragg} = 4.20%, GoF = 4.34. The wavelength was 0.45336 Å.

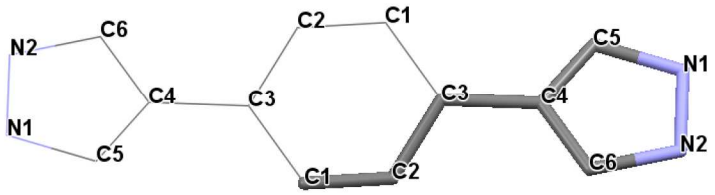

Figure S23. Rigid body description of the linker molecule. The rigid body description of the bdp^{2-} ligand is drawn with bold lines, and the symmetry-generated fragment is drawn with thin lines.

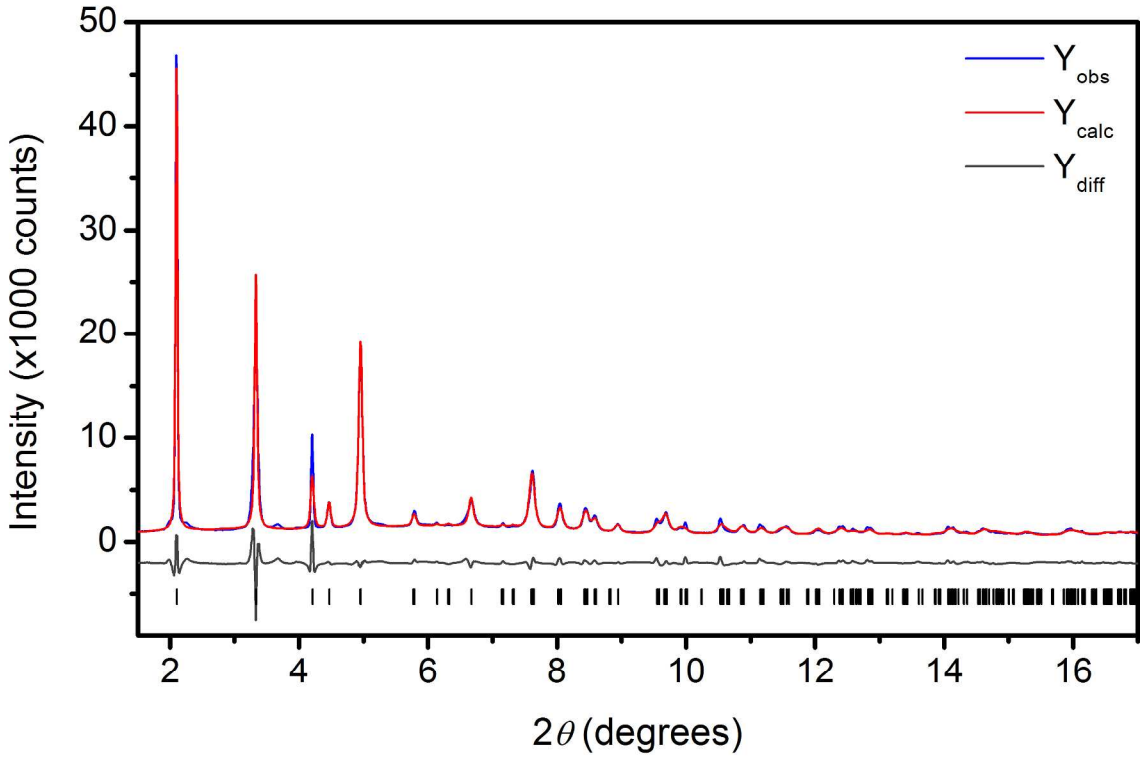

Figure S24. Rietveld refinement of CO_2-dosed Co(bdp). Rietveld refinement of Co(bdp) dosed with 3.6 bar of CO_2 gas at 298 K from 1.5º to 17º. Blue and red lines represent the observed and calculated diffraction patterns, respectively. The gray line represents the difference between observed and calculated patterns, and the black tick marks indicate calculated Bragg peak positions. Figures-of-merit (as defined by TOPAS): R_{wp} = 10.82%, R_p = 7.55%, R_{exp} = 2.56%, R_{Bragg} = 2.57%, GoF = 4.23. The wavelength was 0.45336 Å.

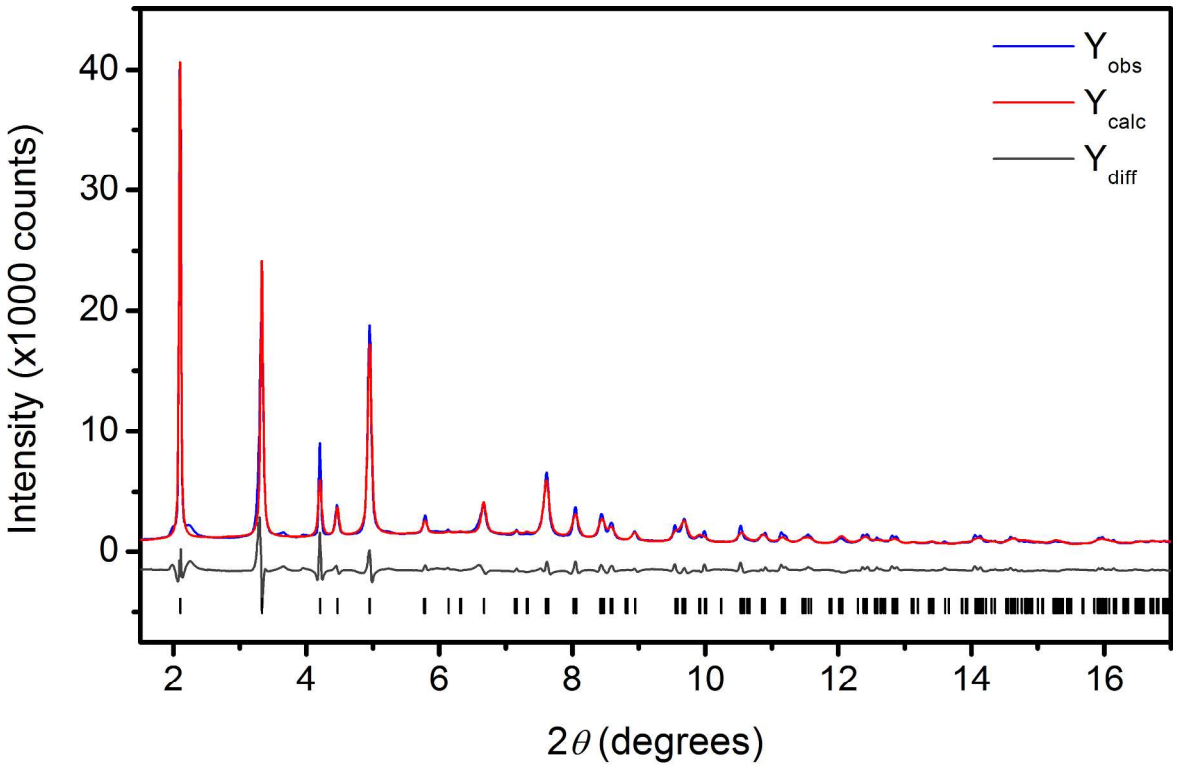

Figure S25. Rietveld refinement of Co(bdp) dosed with mixed gas. Rietveld refinement of Co(bdp) dosed with 7.2 bar of 50:50 CO_2:CH_4 gas at 298 K from 1.5º to 17º. Blue and red lines represent the observed and calculated diffraction patterns, respectively. The gray line represents the difference between observed and calculated patterns, and the black tick marks indicate calculated Bragg peak positions. Figures-of-merit (as defined by TOPAS): R_{wp} = 10.00%, R_p = 6.65%, R_{exp} = 2.50%, R_{Bragg} = 2.09%, GoF = 4.01. The wavelength was 0.45336 Å.

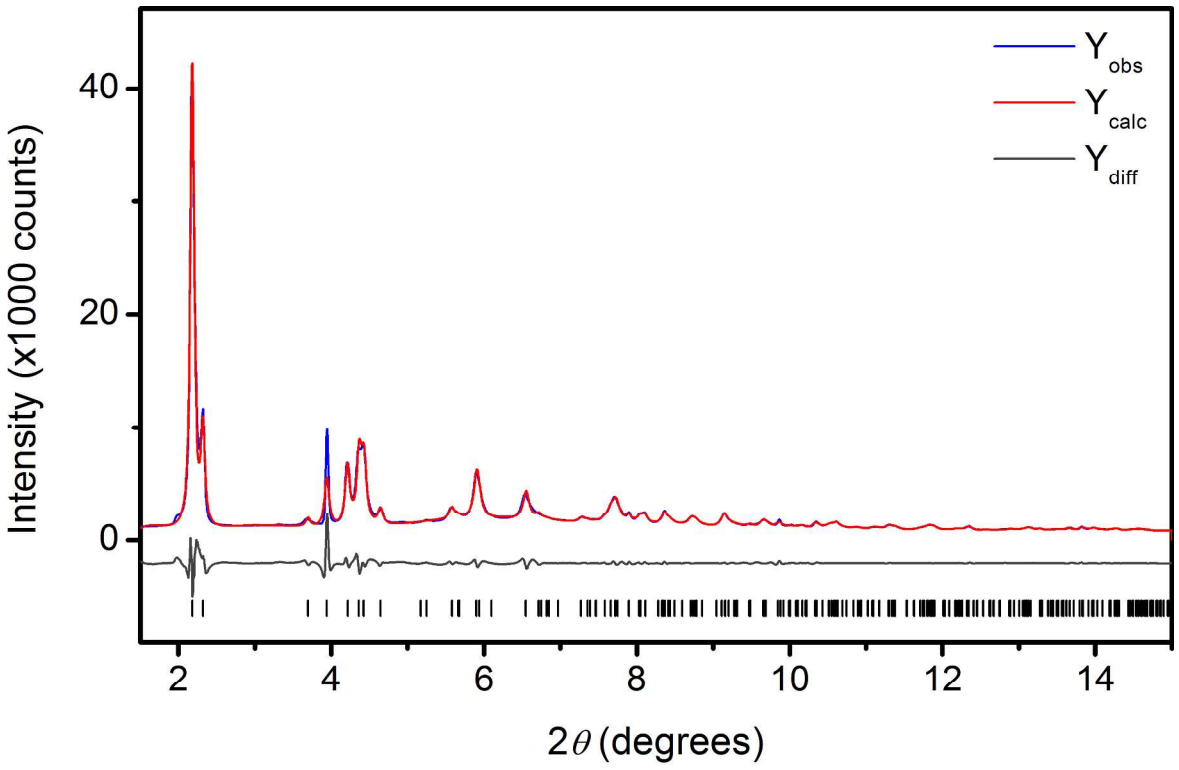

Figure S26. Pawley refinement of CO_2-dosed Co(bdp). The Pawley refinement of Co(bdp) dosed with 11.7 bar of pure CO_2 gas at 298 K from 1.5º to 15º. Blue and red lines represent the observed and calculated diffraction patterns, respectively. The gray line represents the difference between observed and calculated patterns, and the black tick marks indicate calculated Bragg peak positions. Figures-of-merit (as defined by TOPAS): R_{wp} = 7.69%, R_p = 4.32%, R_{exp} = 2.02%, R_{Bragg} = 0.90%, GoF = 3.81. The wavelength was 0.45336 Å.

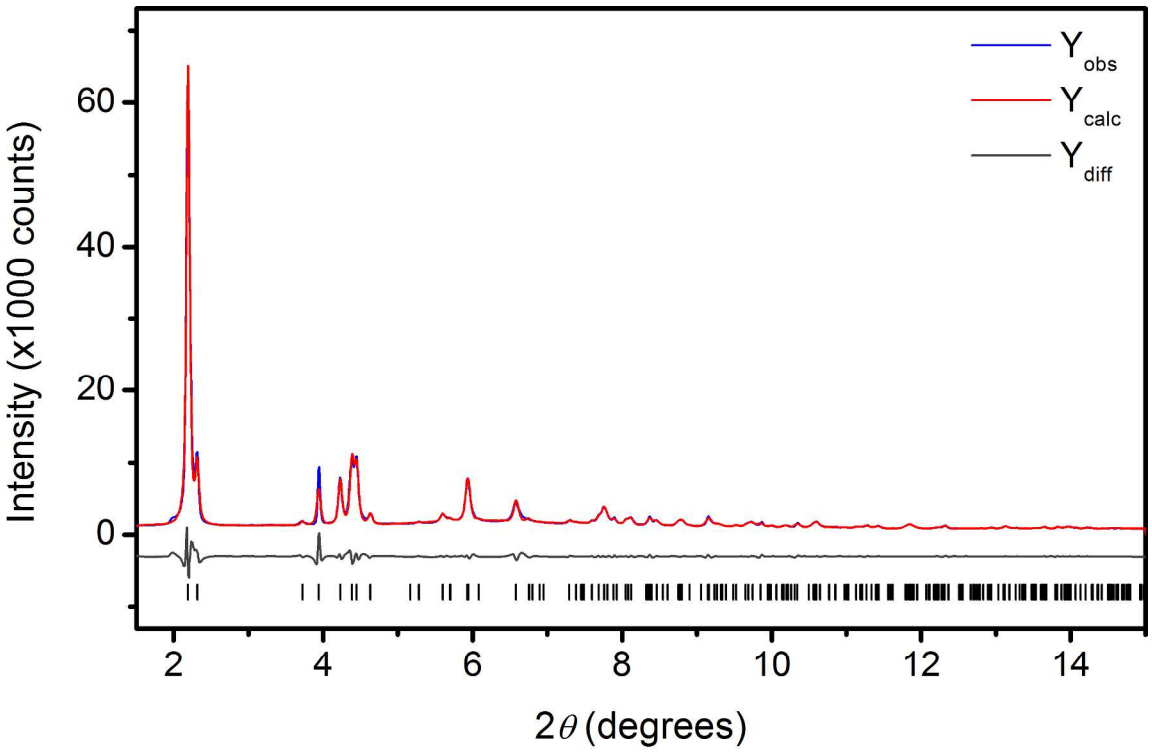

Figure S27. Pawley refinement of Co(bdp) dosed with mixed gas. Pawley refinement of Co(bdp) dosed with 14.9 bar of 50:50 CO_2:CH_4 gas at 298 K from 1.5º to 15º. Blue and red lines represent the observed and calculated diffraction patterns, respectively. The gray line represents the difference between observed and calculated patterns, and the black tick marks indicate calculated Bragg peak positions. Figures-of-merit (as defined by TOPAS): R_{wp} = 7.01%, R_p = 4.30%, R_{exp} = 2.61%, R_{Bragg} = 4.20%, GoF = 3.52. The wavelength was 0.45336 Å.

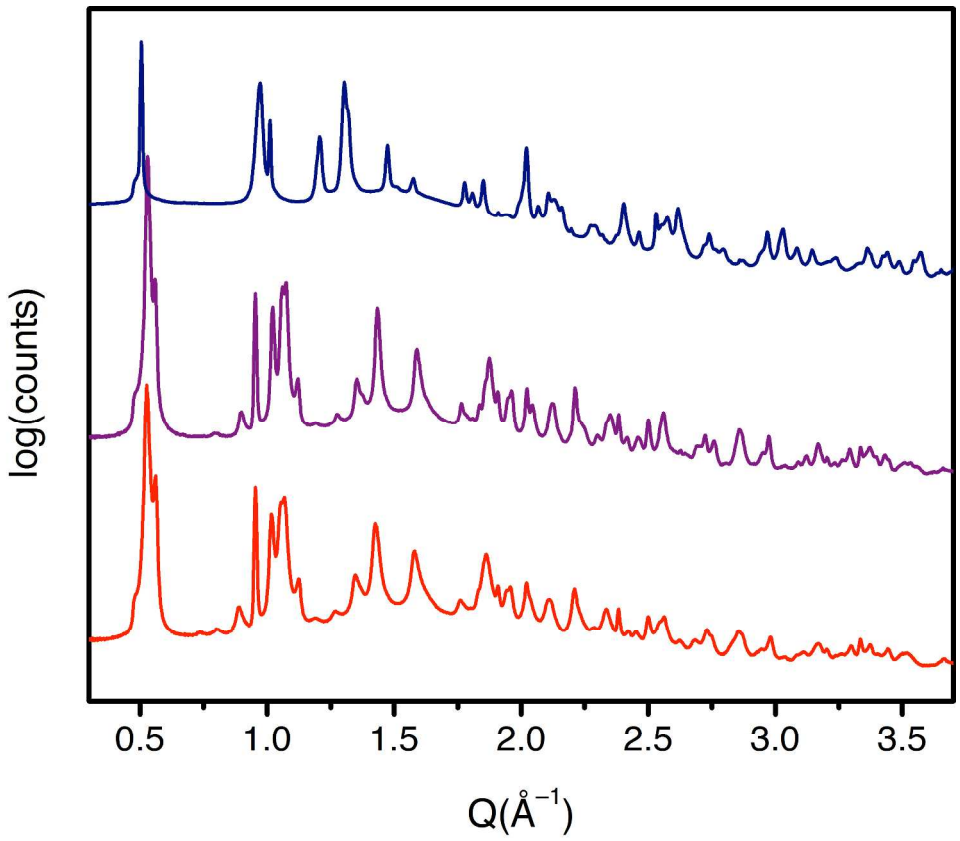

Figure S28. Effect of adsorbate on powder X-ray diffraction data. A comparison of the powder X-ray diffraction data for Co(bdp) dosed with 11.7 bar CO_2 (red), 13.2 bar CH_4 (blue), and 14.9 bar of a 50:50 CO_2:CH_4 mixture (purple) shows that the mixed-gas diffraction pattern closely resembles that of pure CO_2 while the CH_4 data is clearly distinct. The pure CH_4 data was previously published[1]. The pure CH_4 data was collected at a wavelength of 0.75009 Å, the mixed-gas data was collected at 0.45336 Å, and the CO_2 data was collected at 0.45336 Å.

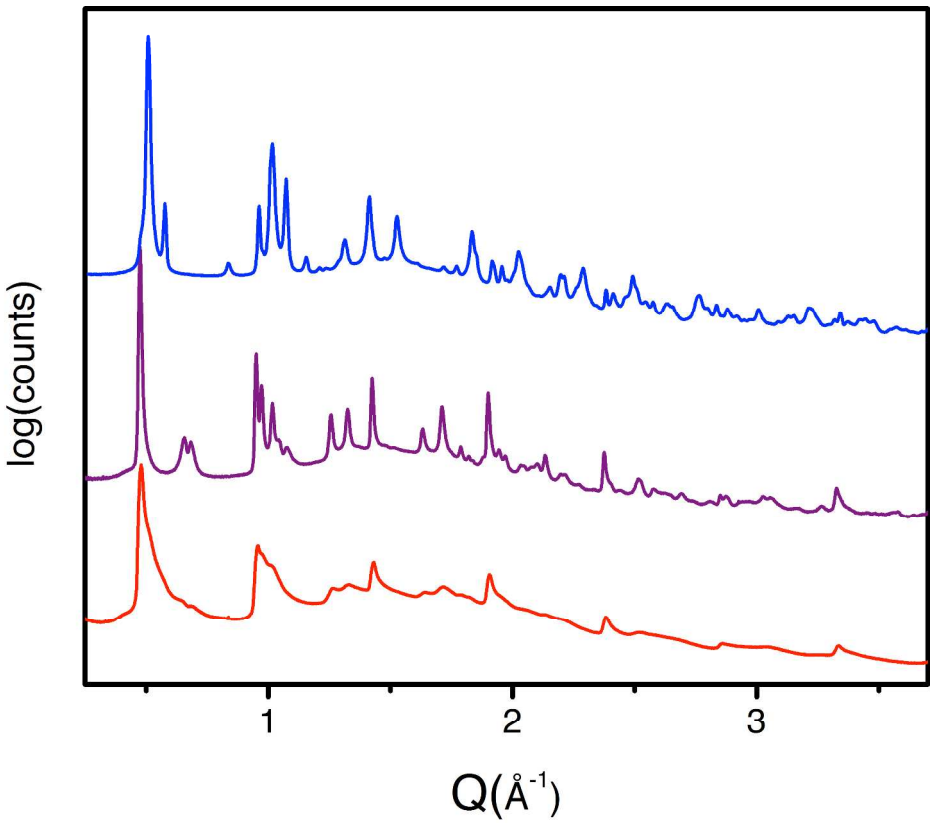

Figure S29. Effect of adsorbate on powder X-ray diffraction data. Powder X-ray diffraction data for Co(bdp) dosed with 29.9 bar CO_2 (red), 23.0 bar CH_4 (blue), and 50.0 bar of a 50:50 CO_2:CH_4 mixture (purple) shows that the the mixed-gas diffraction pattern closely resembles that of pure CO_2, while the CH_4 data is clearly distinct. The pure CH_4 data was previously published[1]. The CO_2-dosed sample displays a great deal of strain at this pressure, as has been seen in other high-pressure gas-dosing experiments in this class of flexible frameworks[1]. The pure CH_4 data was collected at a wavelength of 0.75009 Å, the mixed-gas data was collected at 0.45336 Å, and the CO_2 data was collected at 0.72768 Å.

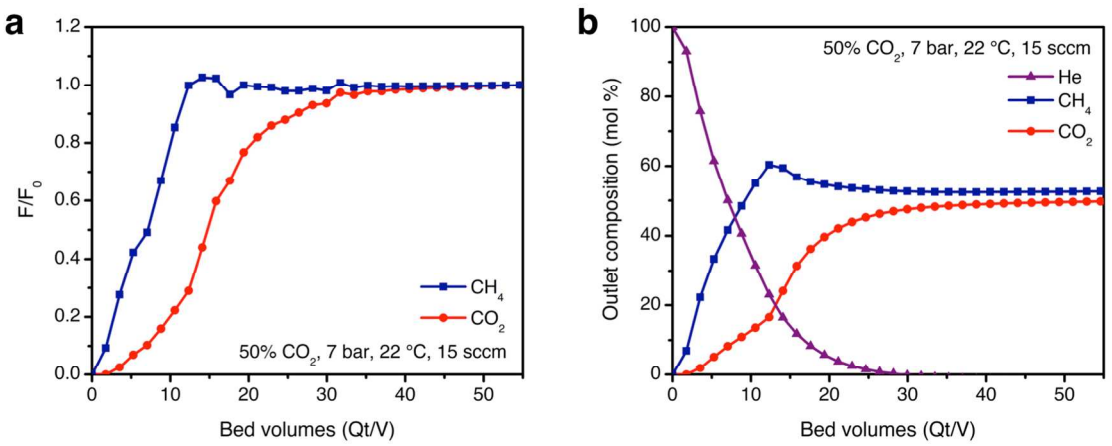

Figure S30. CO_2/CH_4 breakthrough with Co(bdp). Breakthrough of CO_2 (red circles) and CH_4 (blue squares) with Co(bdp) under 15 sccm of 50:50 CO_2:CH_4 at 7 bar absolute pressure and 22 °C. A pressure drop of approximately 0.3 bar was measured across the column. Curves are plotted in terms of **a,** normalized outlet flow rate (F/F_0) and **b,** composition (mol %, right) as a function of bed volumes (Qt/V). Helium composition was calculated as the balance of the calibrated CO_2/CH_4 stream. A CO_2 breakthrough capacity of 3.0 ± 0.3 mmol/g was calculated from this experiment, and the CH_4 breakthrough capacity was within error of zero following correction from the Ar breakthrough curve collected under equivalent conditions. The unusual CO_2 breakthrough profile shown here results from the inability of Co(bdp) to capture CO_2 at partial pressures below the CO_2 phase change pressure (approximately 2 bar at 22 °C, or 29% of the total pressure), a phenomenon has been discussed previously for other flexible frameworks.[13]

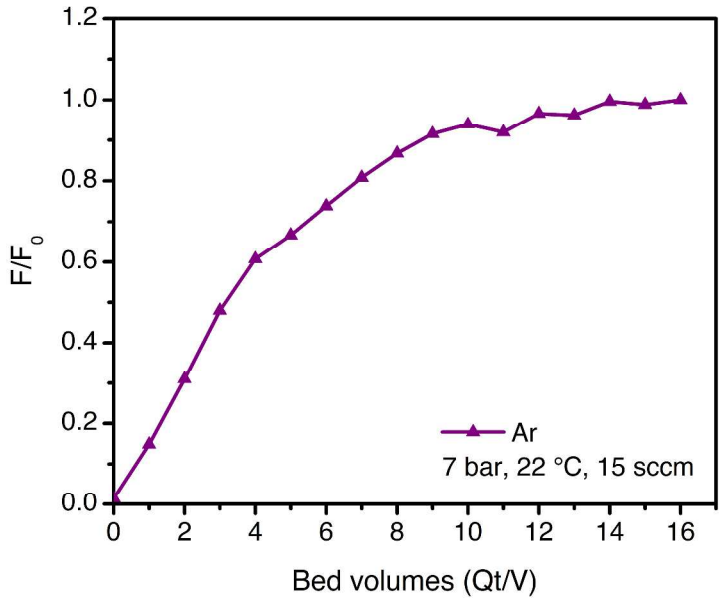

Figure S31. Argon breakthrough with Co(bdp). Breakthrough of Ar (a non-adsorbing probe gas, purple triangles) with Co(bdp) under equivalent experimental conditions as in Figure S30. This curve was used to correct the capacities calculated for the 7 bar experiment reported in Figure S30.

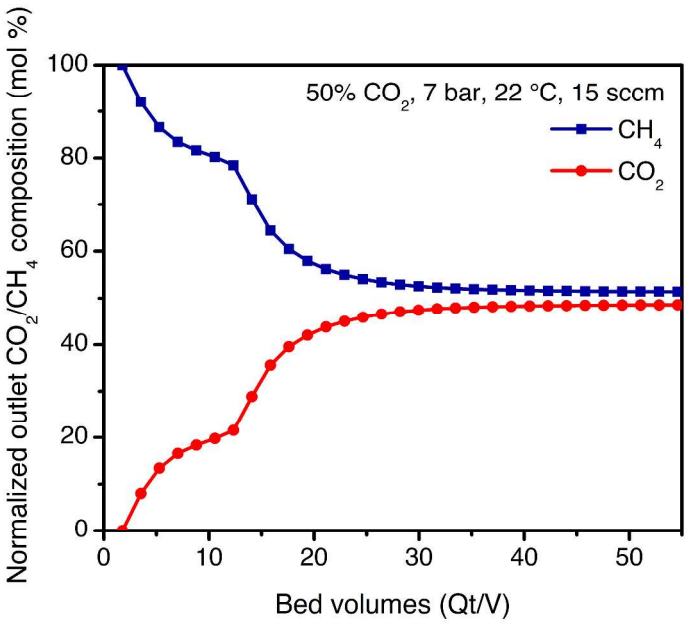

Figure S32. Renormalizing the breakthrough curve in Figure S30 to account exclusively for CO_2 and CH_4 at the outlet suggests the true shape of the breakthrough profile in the absence of He accumulation in the column. Initial "slip" of CO_2 corresponding to the CO_2 step pressure is followed by full breakthrough at saturation. Renormalization was performed by taking the ratio of the calibrated outlet composition of each gas to the sum of the calibrated total CO_2 and CH_4 at the outlet.

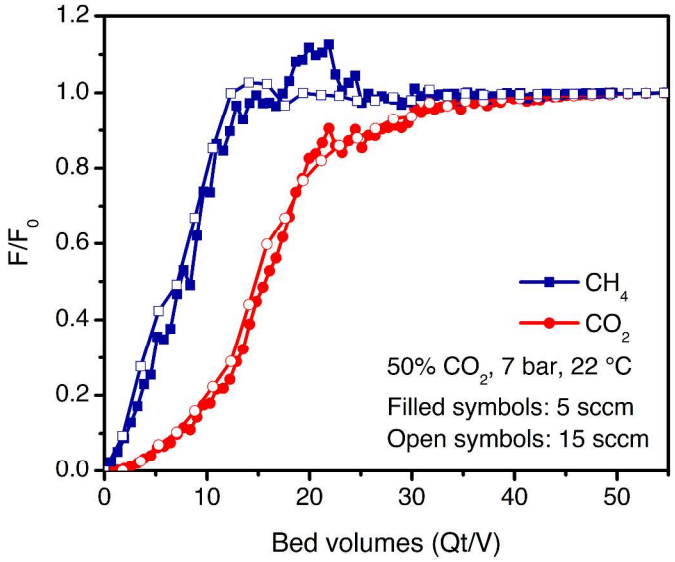

Figure S33. Breakthrough at lower flow rate. Breakthrough of CO_2 (red circles) and CH_4 (blue squares) with Co(bdp) under 50:50 CO_2:CH_4 at 7 bar absolute pressure and 22 °C with a flow rate of 5 sccm (filled symbols). The curves from the equivalent experiment at 15 sccm (Figure S30) are included as open symbols.

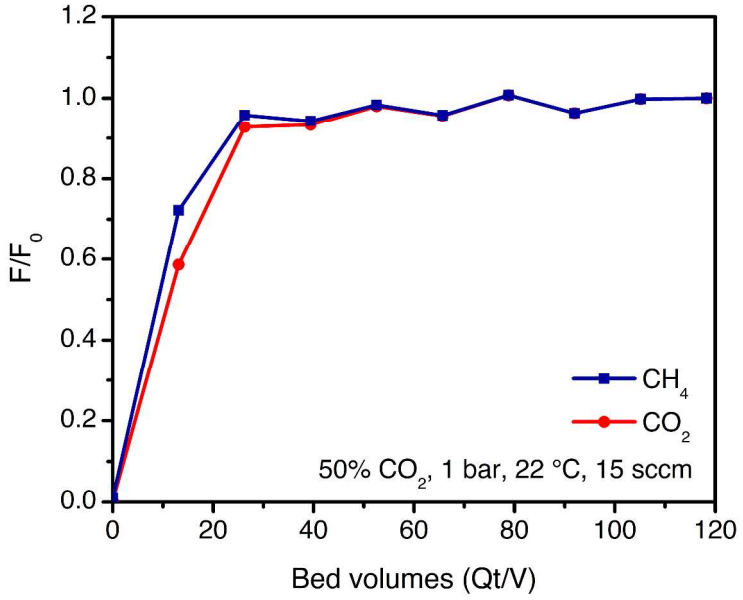

Figure S34. Breakthrough with column exit at atmospheric pressure. Breakthrough of CO_2 (red circles) and CH_4 (blue squares) with Co(bdp) under 15 sccm of 50:50 CO_2:CH_4 at 22 °C with the column exit at atmospheric pressure. A pressure drop of approximately 1 bar was measured across the column. Co(bdp) remains nonporous to both adsorbates under these conditions, and neither gas is retained.

References

1. Mason, J. A.; Oktawiec, J.; Taylor, M. K.; Hudson, M. R.; Rodriguez, J.; Bachman, J. E.; Gonzalez, M. I.; Cervellino, A.; Guagliardi, A.; Brown, C. M.; Llewellyn, P. L.; Masciocchi, N.; Long, J. R. *Nature* **2015**, *527,* 357.
2. H_2bdp was synthesized according to a previously published procedure: Choi, H. J.; Dincă, M.; Long, J. R. *J. Am. Chem. Soc.* **2008**, *130*, 7848.
3. Taylor, M. K.; Runčevski, T.; Oktawiec, J.; Gonzalez, M. I.; Siegelman, R. L.; Mason, J. A.; Ye, J.; Brown, C. M.; Long, J. R. *J. Am. Chem. Soc.* **2016,** *138*, 15019.
4. Kinzel, T.; Yong, Z.; Buchwald, S. L *J. Am. Chem. Soc.* **2010**, *132*, 14073.
5. Smith, J. M.; Van Ness, H. C.; Abbott, M. M. *Introduction to Chemical Engineering Thermodynamics,* 6th ed.; McGraw-Hill: New York, **2003**.
6. Lemmon, E. W.; Huber, M. L.; McLinden, M. O. *NIST Standard Reference Database 23: Reference Fluid Thermodynamic and Transport Properties REFPROP Version 8.0;* National Institute of Standards and Technology: Gaithersburg, MD, **2007**.
7. Bruker AXS, Topas, version 4.1. **2007**.
8. Coelho, A. A. *J. Appl. Cryst.* **2003,** *36,* 86.
9. Pawley, G. S. *J. Appl. Cryst.* **1981,** *14,* 357.
10. Andreev, Y. G.; MacGlashan, G. S.; Bruce, P. G. *Phys. Rev. B* **1997,** *55,* 12011.
11. Rietveld, H. M. *J. Appl. Cryst*. **1969,** *2,* 65.
12. Mercury CSD 3.3 (Build RC5), **2013**.
13. Hiraide, S.; Tanaka, H.; Ishikawa, N.; Miyahara, M. T. *ACS Appl. Mater. Interfaces* **2017,** *9,* 41066.